NASA TECHNICAL
MEMORANDUM

NASA TM X-2016

CASE FILE
COPY

EXPERIMENTAL INVESTIGATION OF A LARGE-SCALE, TWO-DIMENSIONAL, MIXED-COMPRESSION INLET SYSTEM -

Performance at Design Conditions, $M_\infty = 3.0$

by Warren E. Anderson and Norman D. Wong

Ames Research Center
Moffett Field, Calif. 94035

1. Report No. NASA TM X-2016	2. Government Accession No.	3. Recipient's Catalog No.
4. Title and Subtitle EXPERIMENTAL INVESTIGATION OF A LARGE-SCALE, TWO-DIMENSIONAL, MIXED-COMPRESSION INLET SYSTEM - Performance at Design Conditions, $M_\infty = 3.0$		5. Report Date May 1970
		6. Performing Organization Code
7. Author(s) Warren E. Anderson and Norman D. Wong		8. Performing Organization Report No. A-3507
		10. Work Unit No. 720-03-01-01-00-21
9. Performing Organization Name and Address NASA Ames Research Center Moffett Field, Calif., 94035		11. Contract or Grant No.
		13. Type of Report and Period Covered Technical Memorandum
12. Sponsoring Agency Name and Address National Aeronautics and Space Administration Washington, D.C. 20546		14. Sponsoring Agency Code

15. Supplementary Notes

16. Abstract

    Data are presented for a large-scale variable-geometry inlet system operating at the design Mach number of 3.0. Variable features for off-design operation are an adjustable height ramp system and a translating cowl. Total-pressure recovery performance was high, with the maximum being 0.90 for a boundary-layer-bleed mass-flow ratio of 0.146 at α and β equal to $0°$. The effects of boundary-layer bleed, subsonic diffuser shape, throat-mounted vortex generators, and other geometric variables were evaluated experimentally.

17. Key Words (Suggested by Author(s)) Air inlets Total-pressure recovery Boundary-layer-bleed systems Inlet design Vortex generators	18. Distribution Statement Unclassified - Unlimited

19. Security Classif. (of this report) Unclassified	20. Security Classif. (of this page) Unclassified	21. No. of Pages 55	22. Price* $ 3.00

SYMBOLS

A area

A_c inlet capture area (196 in.^{2}), defined at $\alpha = 0°$

A_t inlet throat area, in.^{2}

h height, in.

h_t throat height, in.

h_{t_u} unstart throat height, in.

M Mach number

m_∞ capture mass flow, $\rho_\infty V_\infty A_c$

$\dfrac{m_2}{m_\infty}$ main duct (engine) mass-flow ratio, $\dfrac{\rho_2 V_2 A_2}{\rho_\infty V_\infty A_c}$

$\dfrac{m_{bl}}{m_\infty}$ boundary-layer-bleed mass-flow ratio

p static pressure

p_t total pressure

$\bar{p}_{t_2}$ area-weighted average total pressure at engine-face station

Δp_{t_2} distortion index, $\dfrac{p_{t_2 \max} - p_{t_2 \min}}{\bar{p}_{t_2}}$

$\bar{p}_{t_{bl}}$ area-weighted average total pressure at bleed-duct rake station

$\dfrac{\bar{p}_{t_2}}{p_{t_\infty}}$ main duct total-pressure recovery ratio

V velocity, ft/sec

$\dfrac{V_l}{V_o}$ boundary-layer local velocity ratio (referenced to velocity at h = 1.0 in.)

α angle of attack, deg

β angle of yaw, deg

δ_2 deflection angle of ramp no. 2, from free stream at $\alpha = 0°$, deg

ρ mass density, slugs/ft^3

θ equivalent conical-diffuser half-angle, deg

Subscripts

∞ free-stream conditions

l local

2   engine-face station

Vortex Generator Notation

V   vortex generators (height = 5/8 in., $\alpha = 16°$)

RF   ramp location, forward

RA   ramp location, aft

RFA   ramp location, forward and aft

RCF   ramp and cowl location, forward

(L)   long span (height = 1.0 in.)

EXPERIMENTAL INVESTIGATION OF A LARGE-SCALE, TWO-DIMENSIONAL,

MIXED-COMPRESSION INLET SYSTEM -

Performance at Design Conditions, M_∞ = 3.0

Warren E. Anderson and Norman D. Wong

Ames Research Center

SUMMARY

Advanced supersonic aircraft require highly developed air-induction systems to attain maximum performance. With supersonic transport mission studies as a guideline, a large scale, two-dimensional, mixed-compression inlet model was designed for Mach number 3.0. Overall compression efficiency of the inlet system was investigated over the Mach number range from 0.6 to 3.2. The Reynolds number per foot in this range varied from 4.3×10^6 to 2.0×10^6, respectively.

Data are presented for the design Mach number of 3.0 (Reynolds number per foot = 2.2×10^6) where high inlet performance was obtained. The effects on performance of boundary-layer bleed utilizing porous internal surfaces were investigated extensively. Other geometric variables evaluated included subsonic diffuser shape and vortex generators mounted in the throat region for reduced flow distortion at the engine-face station. Also, the effect of variations in throat region divergence and throat height were investigated. Extensive measurements of boundary-layer profiles on the internal duct surfaces indicated a strong forced mixing effect on the ramp resulting from the use of vortex generators. Engine-face total-pressure performance, diffuser static-pressure distributions, boundary-layer characteristics, and engine-face static-pressure unsteadiness are presented for an optimum diffuser and bleed combination.

INTRODUCTION

The technical disciplines that form the basis for designs of supersonic aircraft must be continually upgraded by extension and revision to meet the expanding needs of present and future design requirements. Although the technology of aircraft propulsion systems in general is a primary concern to designers, air-induction systems specifically have been the focal point of recent aerodynamic interest because of their unique function of controlling the important aerodynamic interface between airframe and engine. The requirement of airframe-engine compatibility extends over an ever increasing flight envelope that places extreme demands on the inlet system. To attain the required levels of air-induction system efficiency over a complete flight

envelope, it is necessary to utilize sophisticated variable-geometry inlets carefully integrated with the overall vehicle design.

Although it remains for specific inlet designs to be developed on the basis of particular aircraft and mission specifications, general research efforts are necessary to determine the level of inlet performance to be applied in the critical early stages of preliminary design and concept definition. Accordingly, an effort has been initiated by Ames Research Center to investigate the overall compression efficiency of a basic two-dimensional, large-scale inlet system designed to meet the relatively high performance levels necessary for both commercial supersonic transport and advanced military strategic aircraft. The system utilizes both external and internal (mixed) supersonic compression surfaces of the variable-geometry type. These surfaces were designed to optimize the shock-wave pattern and internal aerodynamic efficiency in terms of engine-face total-pressure performance at a free-stream Mach number of 3.0. Porous internal surfaces were utilized for boundary-layer bleed control. Preliminary results of tests on the model are presented for a range of Mach numbers in references 1 and 2, and performance information on similar types of systems is contained in references 3 to 9.

Experimental test work was accomplished in the Ames Unitary Plan Wind Tunnel at Mach numbers from 0.6 to 3.2, and a Reynolds number per foot from 4.3×10^6 to 2.0×10^6, respectively. The present report covers design point performance at a free-stream Mach number of 3.0 and a Reynolds number per foot of 2.2×10^6.

MODEL DESIGN CONSIDERATIONS

Supersonic transport mission studies were utilized to establish the guidelines for design of the two-dimensional inlet research model. However, final design and model instrumentation reflect the need to provide basic performance data applicable to a variety of aircraft concepts. Aerodynamic performance was the primary consideration in selecting the final model geometry, although the importance of reduced structural weight was recognized by the limit set on diffuser length.

The aerodynamic merit of an inlet system involves many "tradeoffs" which can best be evaluated in terms of net propulsive efficiency. This factor considers engine net thrust capability, inlet-engine matching drag penalties, and the external drag of the propulsion package.

Net thrust is optimized by high inlet-airflow compression efficiency which is characterized by high total-pressure recovery and low levels of distortion and turbulence at the engine compressor-face station. The attainment of high compression efficiency over a wide range of free-stream Mach numbers dictates the use of variable-geometry compression surfaces and an internal boundary-layer bleed system. A major objective of the present two-dimensional inlet research program was to optimize the location and quantity of boundary-layer bleed flow. Since bleed flow and associated ducting can represent a

2

large drag and weight penalty, determining the tradeoff for bleed quantity in terms of the compression efficiency parameters at design conditions was an important program goal.

Two other drag components that influenced the inlet design were spillage drag and external cowl pressure drag. Low angle external compression surfaces are essential for minimum spillage drag, particularly during transonic flight where spillage mass flow is greatest. To fulfill this requirement a proportionately large amount of internal compression was provided and the external compression angle was limited to 7.0°. As a result of this ramp geometry, the cowl design had low external angles and a small projected frontal area to minimize the external pressure drag.

A desirable feature of any aircraft system is light weight, which for an inlet system is primarily associated with short overall length. Whereas the design length of the supersonic portion of a diffuser is necessarily guided by rigid aerodynamic considerations associated with the shock wave pattern, the design of subsonic diffusers is not so clearly limited. Appreciable gains in vehicle payload performance are associated with short, light-weight subsonic diffusers; however, such diffusers are usually accompanied by intolerable levels of engine-face flow distortion which degrade the thermodynamic performance of the engine. Since insufficient experimental data exist on subsonic diffuser systems for two-dimensional inlets, considerable effort during both design and test was devoted to this aspect of the research program. Included in the testing was the investigation of vortex generators to improve engine-face flow distortion.

Finally, mixed-compression inlet systems must be capable of allowing internal supersonic compression to start at a relatively low supersonic Mach number. An "unstarted" inlet above a local cowl lip Mach number of about 1.5 causes excessive total-pressure losses and spillage drag because of the external position of the terminal shock wave. The problem is one of reducing the geometric contraction ratio of the inlet to a value consistent with a low starting Mach number. For two-dimensional systems either collapsing ramps or a translatable cowl will provide the geometric variation needed. Both methods were utilized on the present model so as not to compromise the overall requirements of (a) matching off-design engine airflow demand, (b) providing a relatively short diffuser and, (3) providing efficient external compression and spillage at low off-design Mach numbers.

MODEL AND APPARATUS

Figure 1 shows the two-dimensional inlet research model installed in the tunnel. Some distinguishing model features are the boundary-layer bleed ducts, shown mounted on the top of the model, the variable-ramp drive mechanism, shown above the sidewall bleed exit ports, and the porous internal surfaces.

Geometric details of the model including installed instrumentation are presented in figures 2 through 10. A drawing of the model, designed for an

3

entrance Mach number of 3.0 is shown in figure 2(a); the theoretical inviscid shock-wave pattern for this condition is shown in figure 2(b). The initial compression ramp is fixed at an angle of 7.0° and the capture height and width are both fixed at 14.0 inches. An adjustable ramp assembly provides the variation in internal contraction ratio required for the range of test Mach numbers. The assembly contains three ramps (ramps 2, 3, and 4 in fig. 2(a)) and is positioned by adjusting the height of the throat ramp (3) which is actuated through a double linkage mechanism. The first movable ramp (2) has a straight-line contour from the hinge line at model station 28.0 to station 54.1 and can be varied through a range of angles (δ_2) from about 6° to 14°. A floating-pin hinge attaches the throat ramp to the aft ramp (4) and provides the length adjustment required during actuation of the ramp assembly. A fixed conical exit plug with translating sleeve is provided to control the main-duct flow. Also, the cowl is translatable through the limits indicated in figure 2(a).

Figure 3 shows the relationship of the second ramp angle to both the duct height and area at the throat station. The area variation in the throat region (divergence) was controlled by the differential movement of the two ramp actuating arms. Curves for the maximum and minimum limits of divergence are noted. To achieve design or normal divergence the ramp system was operated with the arms parallel as shown in figure 2(a). Minimum divergence resulted in a significant displacement of the throat location to a downstream model station (see fig. 4).

Variations of diffuser area ratio[1] are plotted in figure 5 for representative second ramp angles (δ_2) of 7.0°, 10.0°, and 14.0°. At design conditions ($\delta_2 = 14°$), about 60 percent of the supersonic area contraction was accomplished internally. Area-ratio details including the limits of the variable throat divergence for the second ramp design angle of 14° are plotted in figures 6 and 7. Initial tests were completed on a short subsonic diffuser with an equivalent conical-diffuser angle (2θ) of about 9°;[2] however, the maximum local turning angle of the ramp surface was about 26°. Tests indicated the ramp flow was separated in the subsonic diffuser; therefore, the diffuser was redesigned to have a more standard length approximating an equivalent conical angle of 6.5° A relatively minor change was made in engine-face station area. In addition, ramp curvature was modified reducing the maximum local turning angle to about 16°. Complete information on the internal geometry of both the short and standard length diffusers is provided in table 1 for design conditions. Circular-arc fillets provide the transition from the rectangular shaped throat to a circular exit. The intermediate engine-face station appears as a "stretched" circle shape in figure 9.

Details of the boundary-layer-bleed system are shown in figure 8. Variation of the internal bleed distribution was accomplished with a series of replaceable perforated plates with various hole sizes and porosities. Sidewall plates are designated S1 to S6 and the cowl and ramp plates are designated C1 to C3 and R1 to R6, respectively. The ramp boundary-layer bleed flow passed through the perforated plates into three compartmented

---

[1]Area ratio is determined from the local area in a plane normal to the duct centerline.

[2]Average value for full length of subsonic diffuser (see fig. 6).

4

bleed zones (I, II, and III) located above the ramp assembly and separated
by hinged-plate dividers. The sidewall bleed flow associated with zones II
and III was initially ducted through passages within the sidewall structure
and into the compartmented regions. The air was exhausted through circular
ducts to variable area exit plugs (see fig. 2). Some of the bleed flow was
exhausted directly to the ambient airstream through adjustable area exit ports.
Both the forward sidewall bleed (zone I) and all cowl bleed flows were
exhausted in this manner. Compartmentation and division of the boundary-
layer-bleed mass flow as described above was a precaution taken to preclude
flow recirculation due to the longitudinal pressure gradients within the
diffuser.

Subsonic diffuser investigations involved the use of vortex generators
to improve diffusion efficiency. References 10 and 11 provided performance
data for selecting the geometry and location of the vortex generators as
shown in figure 8(c). Vortex generator height and angle of attack were
varied during the investigation.

Flush static-pressure orifices were located along the mid-duct line
of all four internal surfaces and extended to the external lip surfaces of
the cowl and sidewalls. Boundary-layer survey rakes were installed on
ramps 2, 3, and 4 and at two stations on both the cowl and right-hand side-
wall (see fig. 8(a)). Main duct average total-pressure recovery ratio was
determined by area-weighting the engine-face rake total-pressure measurements.
The average recovery was, in turn, used to calculate main duct mass flow by
considering uniform choked flow conditions at the exit plug minimum flow-
area station. A drawing of the engine-face rake assembly is shown in fig-
ure 9. Vertical centerline rakes A and D included extra total-pressure
probes near the duct surfaces to permit better accuracy in defining boundary-
layer profiles. The static-pressure cell indicated in figure 9 was a resis-
tance type with a range of ±25 psi and a good frequency response up to 500 Hz.
Three additional cells were located at forward duct stations as indicated in
figure 8(b). Bleed mass-flow and total-pressure recovery ratios were cal-
culated from rake measurements near the exit of each bleed duct as shown in
figure 10. Porous-plate flow coefficients were also calculated from these
rake measurements and applied in calculating those cowl and sidewall bleed
quantities that were exhausted directly to ambient conditions.

TEST PROCEDURE AND MEASUREMENTS

The electrical actuators that positioned the movable model components
were remotely controlled from a single console. Actuator positions were
indicated by means of either slidewire or rotary type microvoltage potenti-
ometers used in conjunction with calibrated indicator units. The performance
curve of main duct total-pressure recovery ratio versus boundary-layer bleed
mass-flow ratio was established for each model configuration and test condi-
tion. Initially, the model was "started" (terminal shock internal) by open-
ing the exit area and actuating the throat ramp to increase the throat area.
Also, the cowl was retracted to facilitate the starting process, after which

the cowl was repositioned at the forward location and the throat height
decreased until "unstart" occurred. The "unstart" throat height was recorded
and a "restart" sequence initiated. Inlet performance was then measured for
several throat heights up to 10 percent greater than the "unstart" value.
For each throat setting, data points were recorded for a range of terminal
shock wave locations up to the most forward stable position. The main-flow
exit area was adjusted to control the terminal shock wave position in the
throat region.

Pressures were measured with a Scanivalve assembly mounted on the model
which utilized resistance-type pressure transducers. A Beckman recorder
located outside the wind tunnel converted the electrical signals to digital
readouts for about 250 pressure measurements. The sequential readout process
required approximately one minute to complete. Actuator readings for deter-
mining ramp, cowl, and plug positions were also recorded for each data point.

Precision of data was estimated on the basis of the following considera-
tions. The error band of the pressure transducers was obtained by calibra-
tion, and the accuracy of the various other measuring and recording
instruments determined by calibration and consistency of data repeatability.
A number of independent variables (total pressure, duct area, etc.) were
used to calculate mass flow ratios, and an analytical error analysis was made
to account for the accuracy of all variables. The maximum errors were deter-
mined to be the following:

$$M_\infty \qquad \pm 0.005$$

$$m_{bl}/m_\infty \qquad \pm 0.005$$

$$m_2/m_\infty \qquad \pm 0.020$$

$$P_{t_l}/P_{t_\infty} \qquad \pm 0.010$$

$$P_l/P_\infty \qquad \pm 0.400$$

$$\bar{P}_{t_2}/P_{t_\infty} \qquad \pm 0.005$$

RESULTS AND DISCUSSION

Boundary-Layer-Bleed Configurations

A representative number of the boundary-layer-bleed configurations
investigated are identified in table 2. Each configuration is numbered and
a letter key indicates the hole size and porosity of individual plates. Fur-
ther description is provided for those patterns obtained when the holes were
filled in a specified manner to alter the distribution of bleed flow. For
example, the aft portion of ramp plate R2 was filled to prevent flow recir-
culation due to the pressure rise resulting from impingement of the cowl
leading-edge shock wave. Also, the aft half of cowl plate C3 was filled to

prevent excessive bleed flow when the terminal shock wave was moved forward to the position for maximum recovery near the minimum throat station. The triangular patterns utilized for configurations 82 and 83 also represent attempts to reduce bleed flow requirements. Configuration 67 employed an isentropic turn between the initial fixed ramp and variable ramp 2 as indicated in table 2. Coordinates for this turning surface are included in table 1.

The effects of variations in boundary-layer-bleed configuration and subsonic diffuser design are shown in figure 11. Maximum total-pressure recovery and the associated distortion index are plotted against boundary-layer-bleed mass-flow ratio. Bleed-duct throttling plugs and exit-area plates were fixed in the full open position to allow choked flow through the porous plates and thus minimize the possibility of recirculation. All of the configurations for which data are presented achieved maximum performance near theoretical design conditions of the contraction ratio and second ramp angle $(\delta_2 = 14°)$. The throat region divergence was set at either normal or minimum in most cases. Generally, increases in the boundary-layer-bleed mass-flow ratio for a given diffuser increased the values of maximum recovery and reduced the associated distortion. Solid connecting lines have been drawn through the data points for those bleed configurations which were tested with various combinations of diffuser length and vortex generators (24, 52, 54, 59, 67, and 80). The data show that total-pressure recovery was improved when the diffuser length was increased and vortex generators were added. A significant reduction in distortion level, however, was accomplished only when vortex generators were added to the ramp and cowl surfaces in combination with the standard diffuser.[3] A total improvement in distortion index from 0.12 to 0.05 was recorded for bleed configuration 80 as a result of using vortex generators. Overall performance was also high, and unless stated otherwise, the remaining discussion will be concerned only with bleed configuration 80 in combination with the standard diffuser and normal throat divergence.

Engine-Face Performance

Vortex generator effect- Engine-face total-pressure performance is plotted in figures 12 to 14, showing the effects of vortex generators. Total-pressure recovery and distortion index are plotted (fig. 12) against boundary-layer-bleed mass-flow ratio which increases as the terminal shock wave is moved forward toward the throat station. Without vortex generators, the standard diffuser provides relatively high total-pressure recovery, but the distortion index is also high since values greater than 0.10 can cause degradation of engine performance. Engine-face total-pressure contours and profiles for the maximum recovery point (figs. 13 and 14) indicate separated flow on the ramp side of the duct since the wall static pressure was greater than the local total pressure. The flow on the ramp is susceptible to separation because the ramp is curved while the inner cowl surface is nearly straight. To avoid separated flow, four pairs of vortex generators were mounted in a row at the forward ramp location (fig. 8) to force mixing within

---

[3]Vortex generators were not investigated with the short diffuser.

the boundary layer forward of the point of separation. The data of figures 13 and 14 indicate that the flow became completely attached at the engine-face station (80 VRF); consequently, maximum recovery increased from 0.885 to 0.90 and distortion decreased from 0.12 to 0.08 (fig. 12). Boundary-layer-bleed mass-flow ratio remained at about 0.146. Additional mixing of the flow with a second row of vortex generators located downstream did not provide further improvement. Mounting vortex generators on both the cowl and the ramp surfaces, however, did decrease distortion further to 0.05, but caused a small reduction in maximum total-pressure recovery.

Included in figure 12 are the maximum recovery values measured for the axisymmetric[4] and two-dimensional inlets of references 1 and 3, respectively. Both inlets utilized highly developed boundary-layer-bleed systems in the supersonic compression region of the duct similar to the inlet of this report. Performance comparisons of this type require careful consideration of the design limits of the configurations involved. In this case both referenced inlets were designed for theoretical shock-wave losses from 2 to 3 percent less than that of the present inlet. At equal levels of boundary-layer bleed the experimental results reflect these theoretical differences and show the present inlet is about 3 percent low in total-pressure recovery. It is interesting that the two-dimensional model of reference 3 was designed with a very long subsonic diffuser and registered the lowest distortion level of the three designs; whereas the axisymmetric model with a relatively short subsonic diffuser and vortex generators on the centerbody and cowl surfaces provided a higher distortion index than the best configurations of the other two designs.

Engine-face total-pressure contours, such as in figure 13, show the flow to be symmetrical about the vertical centerline, and maximum flow asymmetry is represented by the measurements from the vertical engine-face rake. Total-pressure profiles measured with this rake are plotted in figure 15 for several bleed configurations in combination with various diffuser and vortex-generator arrangements. In all cases the diffuser redesign (standard diffuser) was not, in itself, sufficient to eliminate flow separation at the engine-face station. Vortex generators together with the standard diffuser, however, did allow the ramp flow to remain attached, which reduced the distortion index (see fig. 11). It is possible to speculate on the basis of these data that vortex generators would also have provided similar improvements to the short diffuser.

Various vortex generator configurations were investigated in addition to those for which data are presented in figure 15. Most of these configurations were evaluated at the forward ramp location where measurements show a nominal boundary-layer thickness of 0.25 inch. Height of the vortex generators was varied from 3/8 to 1.0 inch and angle of attack from 12° to 18°. Within the range of the variables tested, the geometry of the vortex generators was not critical for obtaining good subsonic diffuser performance.

Effect of throat region geometry- Figure 16 is presented to show the effect of throat region divergence on engine-face total-pressure performance.

---

[4] Identified as medium length diffuser in reference 1.

8

Normal divergence is compared to maximum, minimum, and intermediate settings of divergence. Normal and minimum divergence provide almost identical performance, with maximum recovery occurring when the terminal shock wave is about at the geometric throat station. As the area downstream of the throat is increased over that for normal divergence, recovery performance is reduced. A loss in maximum recovery of 0.06 is indicated for maximum divergence. For this condition, terminal shock wave Mach numbers were appreciably higher than for normal divergence. As a result, terminal shock wave unsteadiness was increased, preventing the terminal shock wave from reaching the throat before inlet unstart. This reduced the achievable recovery but the distortion index remained unchanged.

The effect of throat height on inlet total-pressure performance is shown in figure 17. Both pressure recovery and distortion are optimized at a throat height (h_t) only 2.8 percent greater than the unstart value (h_{t_u}).[5] The ability to position the terminal shock wave at the throat with such a limited throat-area margin for unstart indicates relatively steady flow was achieved in the throat region. Increasing the throat height to 107 percent of the unstart value decreased the maximum total-pressure recovery and increased the distortion index by approximately 0.02.

Effect of model attitude- The effects of angle of attack and angle of yaw on inlet performance are shown in figure 18. Maximum total-pressure recovery was reduced by 0.005 and 0.02 at 2° and 4° angle of attack, respectively. A reduction of about 0.025 was recorded for an increase in angle of yaw to 2°. Figure 18(a) indicates that changing model attitude increased bleed mass-flow ratio for a given level of recovery. At 4° angle of attack, total-pressure recovery comparable to that at $\alpha = 0°$ was attained with an increase in bleed of about 0.02. Distortion was not generally affected by model attitude. The unstart throat height for $\alpha = 4°$ was 19 percent greater than that for $\alpha = 0°$. This effect is consistent with the results shown in figure 18(b) in which the total-pressure parameters are plotted against main-duct mass-flow ratio. Increasing the inlet angle of attack increases the effective inlet capture area thus providing higher duct mass-flow ratios which are based on the reference capture area at $\alpha = 0°$. The effect is reversed at angles of yaw; duct mass-flow ratio is decreased slightly. For isolated inlet operation it is clear that the variable ramp system must be biased to angle of attack and that optimum inlet-engine matching during angle-of-attack excursions requires a bypass system forward of the engine face station. Underwing inlet installations would effectively shield the inlet from flow angularity at angle of attack. However, the wing flow field would compress the inlet capture airflow and also increase inlet capture mass-flow ratio. Flow bypass in the subsonic diffuser was investigated with the inlet of references 3, 4, and 5 and no adverse distortion effects were experienced.

The sum of the main-duct mass-flow ratio and bleed mass-flow ratio from figure 18 indicates about 1.5 percent of the capture mass flow was spilled

---

[5]The unstart value was determined with the terminal shock wave initially located downstream of the throat region (supercritical operation).

forward of the lip leading edge at $M_\infty = 3.0$ and $\alpha = 0°$. Schlieren photographs indicate the external shock wave did lie slightly forward of the lip at these conditions.

<p style="text-align:center">Diffuser Measurements</p>

Boundary-layer bleed- Performance for bleed configuration 80 is presented in figure 19. The individual and total bleed mass-flow ratios are shown plotted against main-duct total-pressure recovery, which varies with terminal shock-wave location. Forward bleed flows (zones I and II) are unaffected by movement of the terminal shock wave toward the minimum throat station; however, throat bleed (zone III) is increased from a total of 0.045 to about 0.07. Nearly all the increase is provided by the sidewalls plus ramp as a result of high porosity sidewall bleed surfaces. Total duct bleed mass-flow ratio is increased from about 0.12 to 0.146. It is of interest to note the values of total-pressure recovery measured for the individual bleed ducts which correspond to the bleed zone mass-flow ratios plotted in figure 19.[6] Bleed ducts 1 and 2 operated with constant recovery values of 0.04 and 0.12, respectively. The operating total-pressure recovery of bleed duct 3 varied from 0.11 for positions of the terminal-shock wave downstream of bleed zone III to 0.17 at the critical operating condition. The increase is associated with the static-pressure rise across the terminal shock wave. This rise represents an increase in total pressure for the throat region boundary-layer flow which is bled through the perforated surface plates and is eventually exhausted by bleed duct 3.

Static-pressure distributions- Local static-pressure ratios measured along the internal surfaces of the inlet model are shown plotted in figure 20. Also noted on the figure are various geometric features together with boundary-layer rake locations. The curves are identified by the corresponding engine face total-pressure recovery values plotted in figure 12. Static-pressure distributions on the ramp, cowl, and sidewall surfaces in the supersonic diffuser agree well with theoretical values obtained from two-dimensional, inviscid, wedge-flow relationships. The maximum recovery conditions both with and without vortex generators occurred with the terminal-shock wave located essentially at the minimum throat station. In the region downstream of the throat the vortex generators provide a slight change in ramp static-pressure ratio and increase the static-pressure recovery at the engine-face station. This change is relatively small considering the large improvement in distortion evident in figures 12 to 14. The sidewall distributions of figure 20(b) for maximum recovery show a constant static pressure immediately downstream of bleed zone III, which suggests local flow separation. This characteristic is evidence of boundary-layer bleed recirculation, which is due to excessive porosity of the sidewall boundary-layer bleed plates in the throat region.

Boundary-layer characteristics- Boundary-layer profiles measured on the ramp, cowl, and sidewall surfaces[7] are presented in figures 21 through 23.

---

[6]Bleed duct 1 handled zone I ramp bleed, bleed ducts 2 and 3 handled ramp plus sidewall bleed for zones II and III, respectively.
[7]Rake locations are indicated on figure 8(a).

10

Ramp surface measurements at upstream, throat, and downstream locations are plotted in figure 21 as total-pressure, Mach number, and velocity profiles. The boundary-layer thickness measured along the ramp surface was uniformly about 0.25 inch. Throat region total-pressure ratios indicate a core flow recovery of about 0.94 as compared with the theoretical design shock-wave recovery value of 0.950. The corresponding theoretical throat Mach number is about 1.2. (See fig. 2(b).) The experimental Mach number distribution in the throat region, however, indicates a value only slightly greater than unity (see $\bar{p}_{t_2}/p_{t_\infty}$ = 0.782), which is unreasonably low. Throat Mach numbers from 1.1 to 1.2 would be more consistent with the ratio of throat height to unstart throat height for which the data are presented (indicated as 1.028 in fig. 17). Surface and rake static pressures were used to compute the Mach number profiles in figure 21(b). These pressures are difficult to measure accurately in the throat region during supercritical operation because of flow angularity and reflecting shock waves. Thus, a Mach number discrepancy is not unexpected. The velocity profiles shown for the downstream ramp location (fig. 21(c)) provide a clear comparison of the effectiveness of vortex generators. Low energy nearly separated flow is eliminated by the forced-mixing process created upstream by the vortex generators and replaced by a more strongly attached boundary-layer profile. As a result, flow conditions at the engine face were improved as discussed earlier.

A representative number of boundary-layer profiles measured at the upstream and throat locations on the sidewall and cowl surfaces are shown in figures 22 and 23, respectively. The ramp mounted vortex generators do not appreciably affect the cowl or sidewall profiles. The boundary-layer thickness on the cowl surface in the throat region is comparable to that on the sidewall although of lower displacement thickness. Both of these boundary layers are considerably thicker than that on the ramp. Again, throat region Mach number profiles on the two surfaces for $\bar{p}_{t_2}/p_{t_\infty}$ = 0.782 indicate low supersonic values but both are somewhat higher than the values measured on the ramp.

Engine-face total-pressure distributions- Figures 24 and 25 present engine-face centerline total-pressure profiles and total-pressure contour maps, respectively, for the flow conditions represented in figures 20 to 23. Separated nonuniform flow is indicated on the ramp for the supercritical flow condition ($\bar{p}_{t_2}/p_{t_\infty}$ = 0.782) characterized by the terminal-shock wave being located downstream of the throat boundary-layer bleed zone. The distortion index value for this operating condition is 0.22 as indicated by the curve in figure 12. As the terminal-shock wave is moved near the throat for maximum total-pressure recovery, separated flow is eliminated, thus lessening distortion and improving flow uniformity at the engine-face station.

Flow unsteadiness- Oscillograph records of typical diffuser static-pressure cell (transducer) measurements are shown in figure 26. Pressure cell locations are indicated in figures 8(b) and 9. The maximum recovery condition occurs with the terminal shock wave located slightly forward of the throat pressure cell (2); consequently, this cell measures appreciable unsteadiness in both the short and standard length diffusers. The amplitude of the pressure fluctuations for the standard diffuser is about 8 percent of

the free-stream total pressure compared to slightly less than 3 percent for the short diffuser. Slight differences in terminal shock-wave location could easily account for this difference. Steady flow conditions exist at the engine face (cell 4) during operation at maximum recovery for both diffusers. During operation in the unstarted mode the throat region again has the greatest unsteadiness (up to 0.254 p_{t_∞} for the short diffuser). The engine-face station (cell 4), however, experiences fluctuations on the order of 9 to 18 percent of the free-stream total-pressure value, which is considered low for conditions of inlet unstart.

CONCLUDING REMARKS

The results of an experimental investigation of a large-scale two-dimensional mixed-compression inlet system are presented for an inlet design Mach number of 3.0. Variable geometry features of the system for off-design operation are an adjustable ramp system and a translating cowl. Porous internal surfaces on the ramps, sidewalls, and cowl are provided for boundary-layer bleed control. The effects of subsonic diffuser shape, throat region divergence, and throat height were investigated. The utilization of a modified subsonic diffuser in combination with vortex generators mounted in the throat region and an optimized boundary-layer-bleed configuration provided high total-pressure performance with low distortion at the compressor-face station. At the design Mach number a total-pressure recovery of 0.90 was obtained for a boundary-layer-bleed mass-flow ratio of 0.146 at angle of attack and angle of yaw equal to zero. Increasing α to 4° or β to 2° resulted in a loss in recovery of about 0.02; however, engine-face distortion remained low. Boundary-layer profiles were measured on the internal duct surfaces and indicated that both sidewall and cowl boundary layers were thicker than those on the ramp surface. Profiles measured on the ramp surface in the subsonic diffuser indicated that a strong forced-mixing effect resulted from the use of vortex generators. As a consequence, separated flow at the engine-face station was replaced by an attached boundary layer, and maximum recovery was increased. Static-pressure unsteadiness was found to be most severe in the terminal-shock-wave region of the throat. Unsteadiness was not evident at the engine-face station during normal inlet operation. During unstart conditions, however, measurements of static-pressure fluctuations up to 18 percent of the free-stream total pressure were obtained at the engine-face station.

Ames Research Center
    National Aeronautics and Space Administration
        Moffett Field, Calif., 94035, Feb. 10, 1970

REFERENCES

1. Sorensen, Norman E.; Anderson, Warren E.; Wong, Norman D.; and Smeltzer, Donald B.: Performance Summary of a Two-Dimensional and Axisymmetric Supersonic Inlet System. NASA TM X-1302, 1966.

2. Anderson, Warren E.; Petersen, Martine W.; and Sorensen, Norman E.: An Evaluation of Transonic Spillage Drag Based on Test Results From Large-Scale Inlet Models. NASA SP-124, 1966, pp. 171-184.

3. Bowditch, David N.; and Anderson, Bernhard H.: Investigation of the Performance and Control of a Mach 3.0 Two-Dimensional External-Internal-Compression Inlet. NASA TM X-470, 1961.

4. Chew, W. L.; and Daniel, B. R.: Wind Tunnel Investigation of the 0.577-Scale B-70 Inlet. AEDC-TDR-62-244, Jan. 1963.

5. Butler, C. B.; Graham, F. J.; Hartin, J. P.; and Daniel, B. R.: Investigation of the 0.25-Scale B-70 Variable-Geometry Inlet at Mach Numbers From 0.60 to 1.40. AEDC-TN-61-72, July 1961.

6. Gertsma, Laurence W.: Effect on Inlet Performance of a Cowl Visor and an Internal-Contraction Cowl for Drag Reduction at Mach Numbers 3.07 and 1.89. NASA MEMO 3-18-59E, 1959.

7. Connors, James F.; and Anderson, Leverett A., Jr.: A Two-Dimensional External-Internal-Compression Inlet With Throat Bypass at Mach 3.05. NASA MEMO 10-3-58E, 1958.

8. Gertsma, L. W.; and Beheim, M. A.: Performance at Mach Numbers 3.07, 1.89, and 0 of Inlets Designed for Inlet-Engine-Matching up to Mach 3. NACA RM E58B13, 1958.

9. Wollett, Richard R.; and Connors, James F.: Zero-Angle-of-Attack Performance of Two-Dimensional Inlets Near Mach Number 3. NACA RM E55K01, 1956.

10. Taylor, H. D.: Application of Vortex Generator Mixing Principle to Diffusers. Concluding Report, R-15064-5, United Aircraft Corp., Research Dept., Dec. 31, 1948.

11. Taylor, Harlan D.: Summary Report on Vortex Generators. Rep. R-05280-9, United Aircraft Corp., Research Dept., March 7, 1950.

TABLE 1.- DESIGN COORDINATES, $\delta_2 = 14°$.

(a) INLET WITH STANDARD DIFFUSER

MODEL STATION	HEIGHT STATION RAMP SURFACE	HEIGHT STATION COWL SURFACE	DUCT HEIGHT	DUCT WIDTH	FILLET RADIUS RAMP SURFACE	FILLET RADIUS COWL SURFACE
0	0	*		14.00		
28.00	3.438	14.00				
30.40	*					
54.11	9.954					
55.00	10.158					
56.00	10.367					
57.00	10.533					
58.00	10.615					
58.80	10.645		3.355			
60.28			3.355			
61.76			3.368			
63.24			3.394			
64.72			3.432			
65.52	10.544	*	3.456			
66.50			3.482			
67.85			3.535			
69.52			3.632			
71.12			3.763			
72.00	10.147		3.853	*		
73.74		13.80	3.92			
74.50			*			0
77.62			4.31			.29
80.00	9.19		4.61			.56
81.52			4.82		0	.76
82.50			4.97		.15	.91
85.00	8.40		5.40		.58	1.29
87.50			5.89		1.09	1.80
90.00	7.36		6.44		1.62	2.39
92.50			7.04		2.22	2.92
95.52	5.94		7.86		3.04	3.50
97.50			8.40		3.58	3.84
99.33			8.86		4.03	4.11
101.36	4.52	13.86	9.34		4.48	4.38
102.50		13.91	9.59		4.69	4.53
105.00	3.92	14.08	10.16		5.08	4.91
107.28		14.38	10.76		5.38	5.38
110.00	3.26	*	11.48		5.74	5.74
113.02			12.28	12.80	6.14	6.14
115.02	2.60	15.40	12.80	12.80	6.40	6.40

(b) INLET WITH SHORT DIFFUSER

MODEL STATION	HEIGHT STATION RAMP SURFACE	HEIGHT STATION COWL SURFACE	DUCT HEIGHT	DUCT WIDTH	FILLET RADIUS RAMP SURFACE	FILLET RADIUS COWL SURFACE
UPSTREAM OF MODEL STATION 72.00, CONTOUR SAME AS THAT FOR THE INLET WITH STANDARD DIFFUSER						
72.00	10.147	14.00 / *	3.853	14.00		
74.50	9.67	13.80	4.130		0	0
75.76			4.400			.114
77.52	8.96		4.840		.147	.290
80.00			5.160		.381	.565
81.52	7.56		5.645		.555	.757
83.52			6.240		.845	1.040
85.52			7.180		1.252	1.381
88.00	5.918		7.882		1.966	1.925
89.52			7.940		2.580	2.363
89.64		13.844	*		2.630	
91.30		13.952	8.487		3.172	2.882
92.48		14.262	9.272		3.573	3.215
93.90	4.256		9.696		4.015	3.633
95.36		14.60 / *	10.482		4.414	4.097
98.25			11.210		5.061	4.980
99.33	3.39		*	*	5.269	5.240
101.28		15.40 / *	11.210		5.605	5.605
109.12	2.60		12.800	12.80	6.400	6.400

All dimensions are in inches

* Straight line between points

(c) ISENTROPIC SURFACE

MODEL STATION	HEIGHT STATION RAMP SURFACE
0	0 / *
18.20	2.235
19.60	2.411
21.00	2.603
22.39	2.805
23.78	3.019
25.17	3.245
26.56	3.484
27.95	3.736
29.33	3.997
30.71	4.273
32.09	4.559
33.47	4.857
34.84	5.169
36.21	5.492
37.58	5.826 / *
54.14	9.954

TABLE 2.- BOUNDARY-LAYER-BLEED CONFIGURATIONS

BLEED CONFIG. NO.	RAMP PLATES						SIDEWALL PLATES						COWL PLATES			
	1	2	3	4	5	6	1	2	3	4	5	6	1	2	2X	3
24	A	A	A	C	S	S	A	A	A	A	S	S	A	A	S	A
52			A	C					A					A		
54			B	C					B							
59				A												
67	Is A			C												
77	A	C											S			
78																S
79								C								A
80								A								C
81		S														C
82		C														
83				C												
84						A										C
85						S				A				S		
86	A									A				A		
87	A		A							A				A		

A   0.125 in. diameter holes, 13% porosity

B   0.125 in. diameter holes, 19.6% porosity

C   0.078 in. diameter holes, 7.6% porosity

S   Soild or blank plate with zero porosity

Is   Isentropic surface

Aft 4 in. of plate holes filled

Aft-half of plate holes filled

Fwd-half of plate holes filled

Every other two rows of holes filled

Plate holes filled in triangular pattern

Plate holes filled in pattern denoted
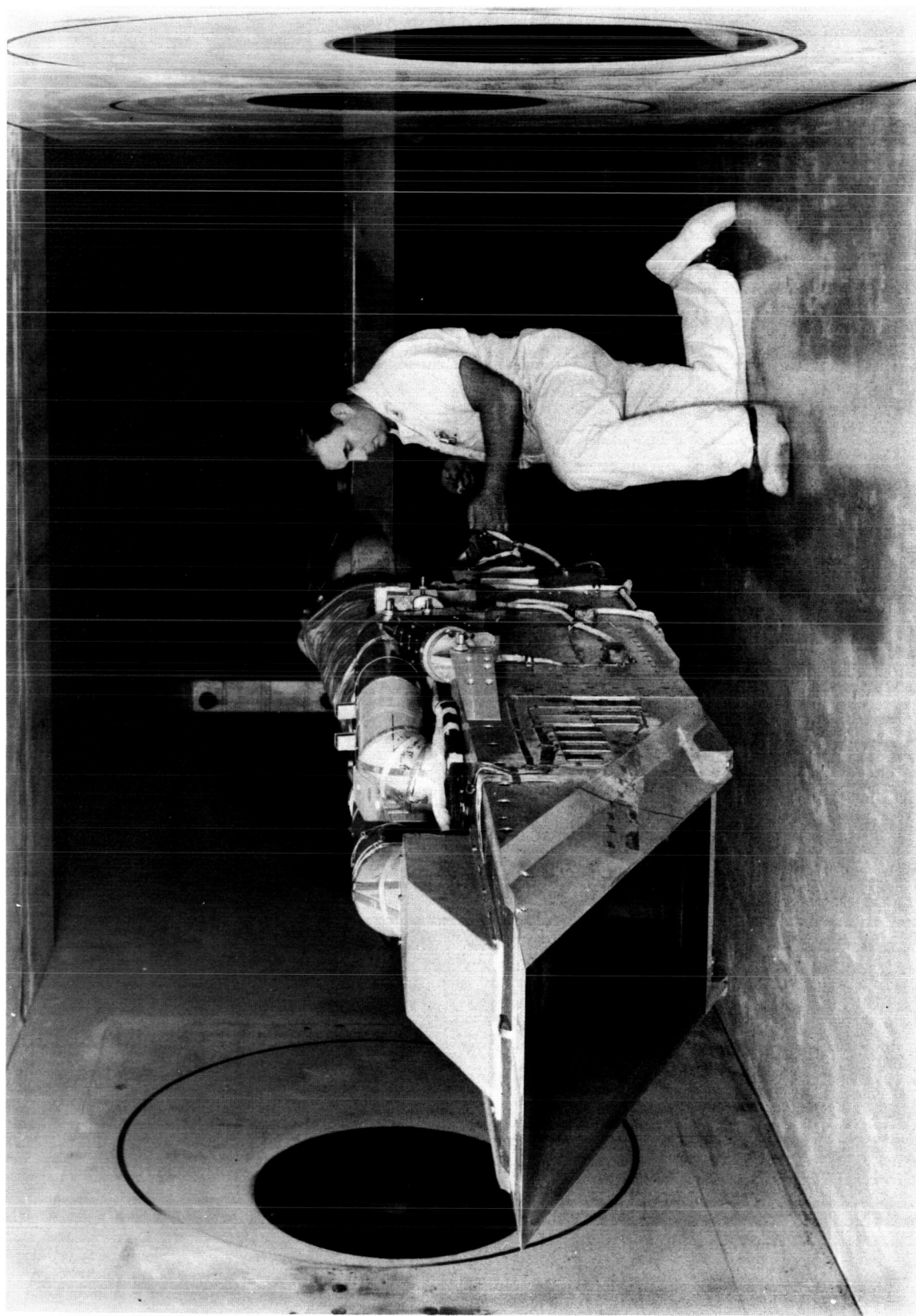
Figure 1.- The two-dimensional inlet research model installed in the Ames Unitary Plan Wind Tunnel.

A-32238

17

Notations I, II, and III are
for the three sidewall and
ramp bleed zones

Note: All dimensions
are in inches
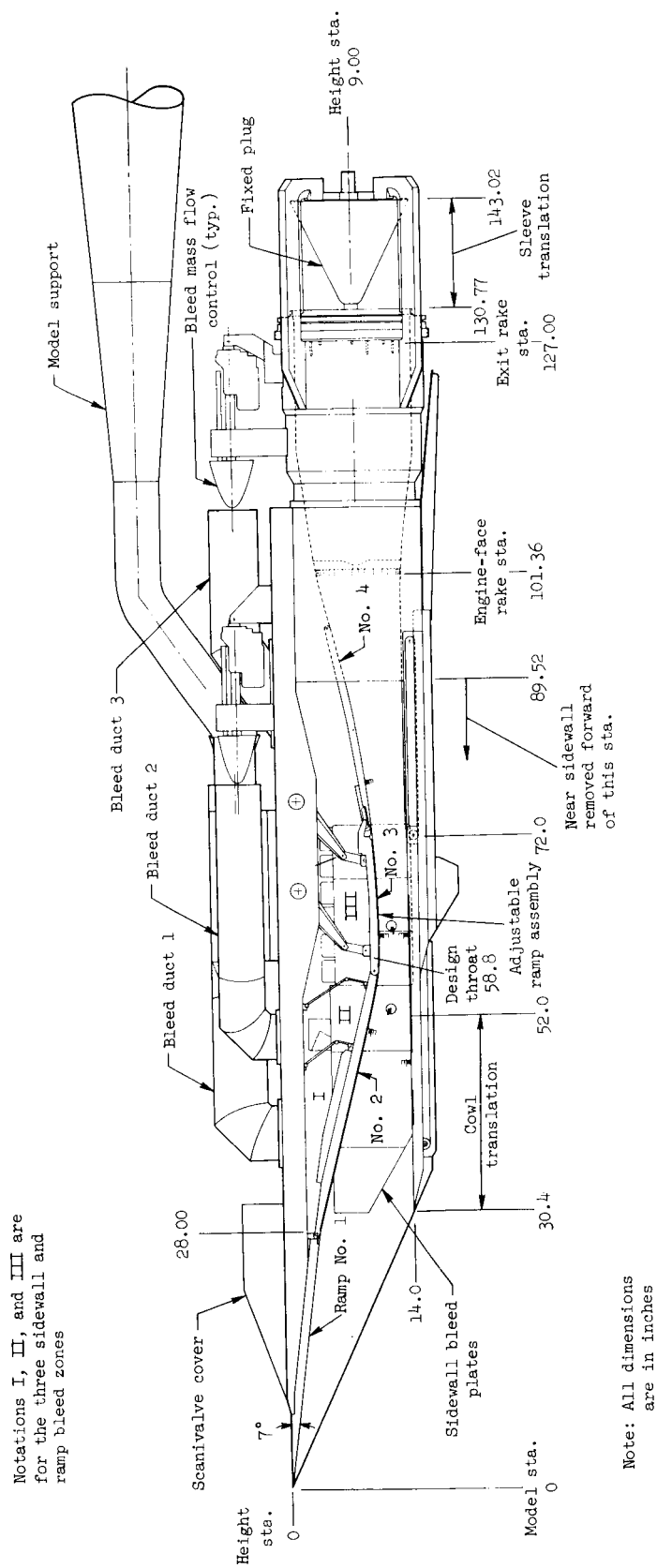
(a) Model drawing, standard diffuser.

Figure 2.- Geometry of the two-dimensional inlet research model.

18

(b) Design inviscid shock-wave pattern.

Figure 2.- Concluded.
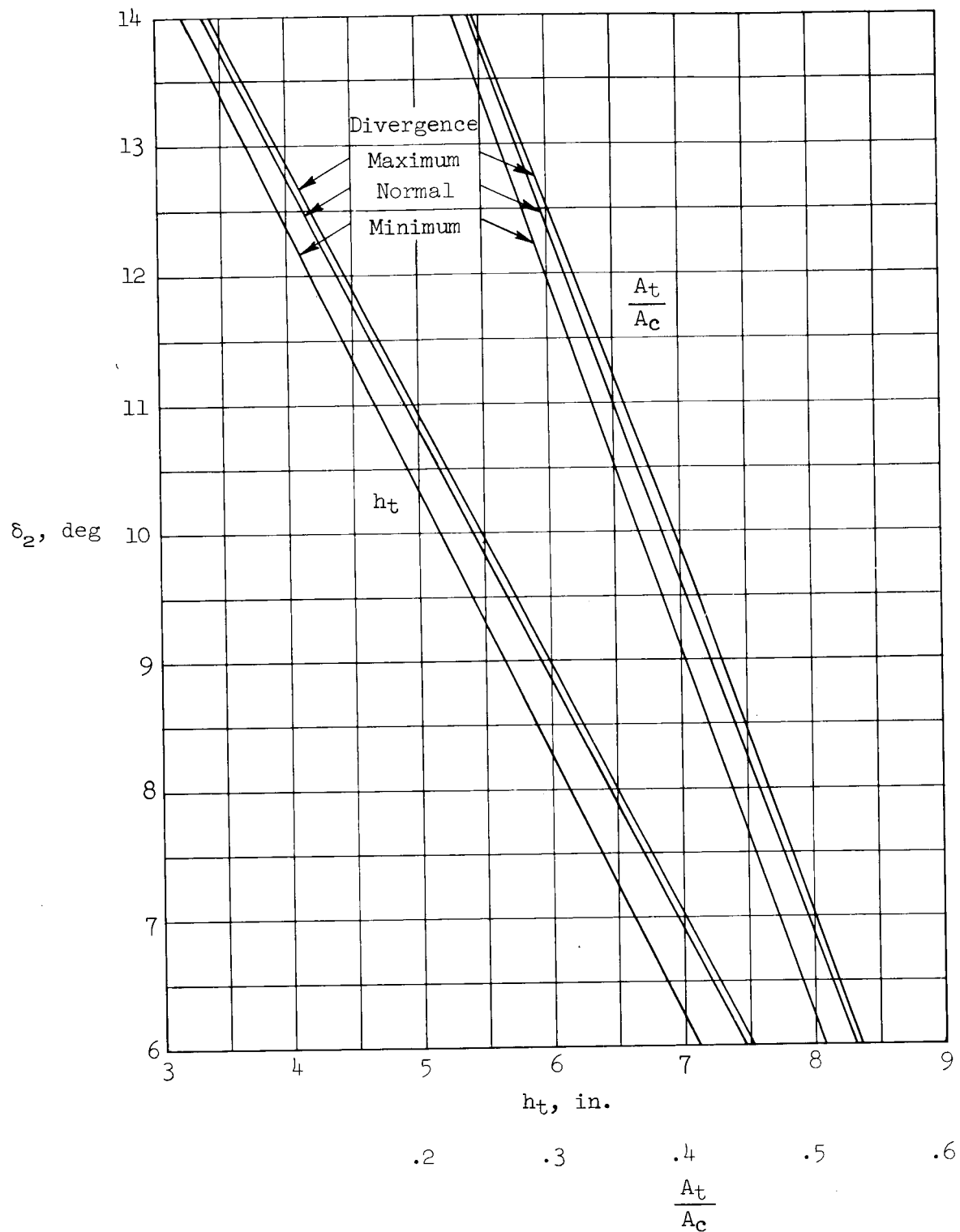
Figure 3.- Relationship of second ramp angle to height and area ratio at the throat station.
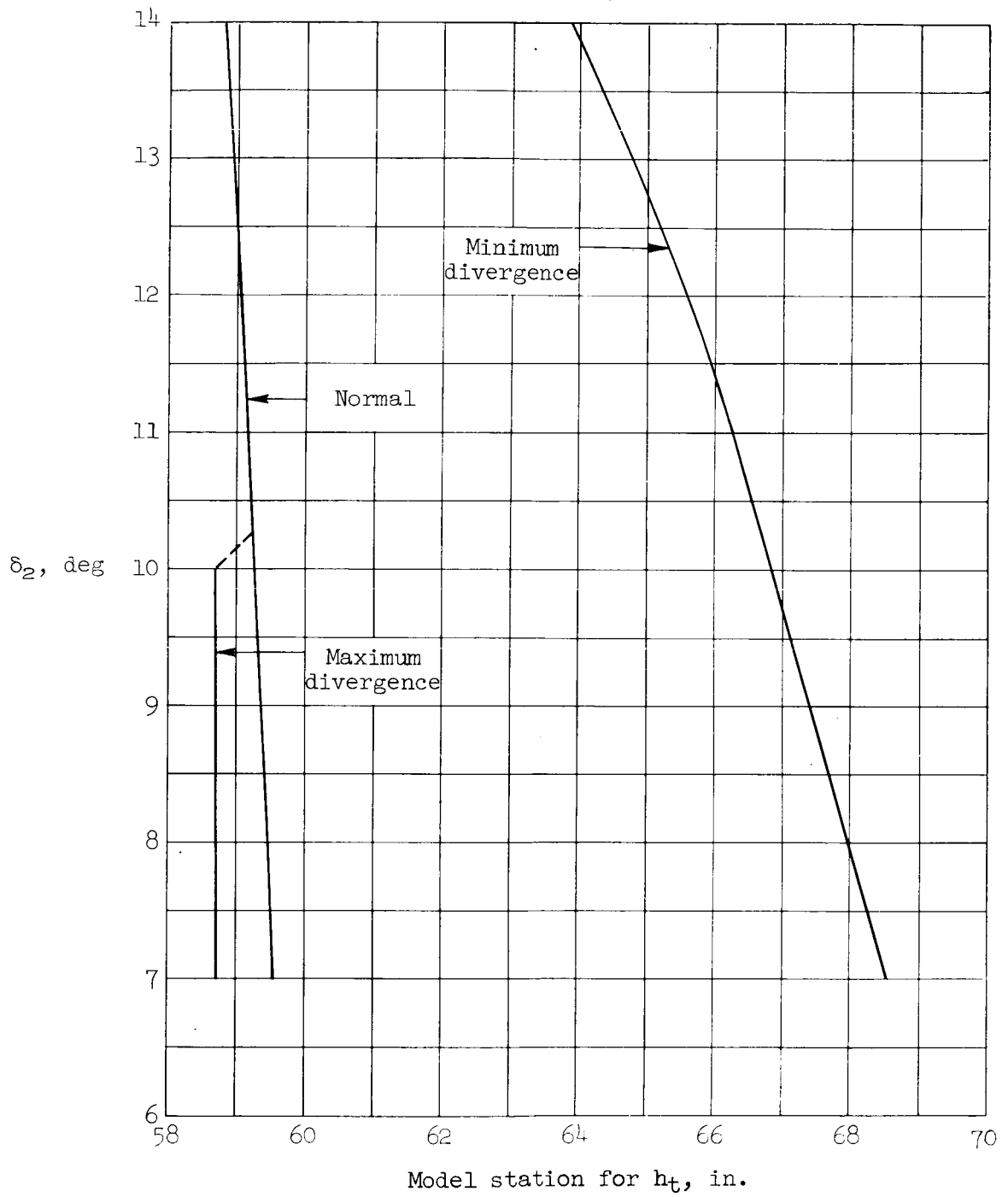
Figure 4.- Relationship of second ramp angle to throat location.
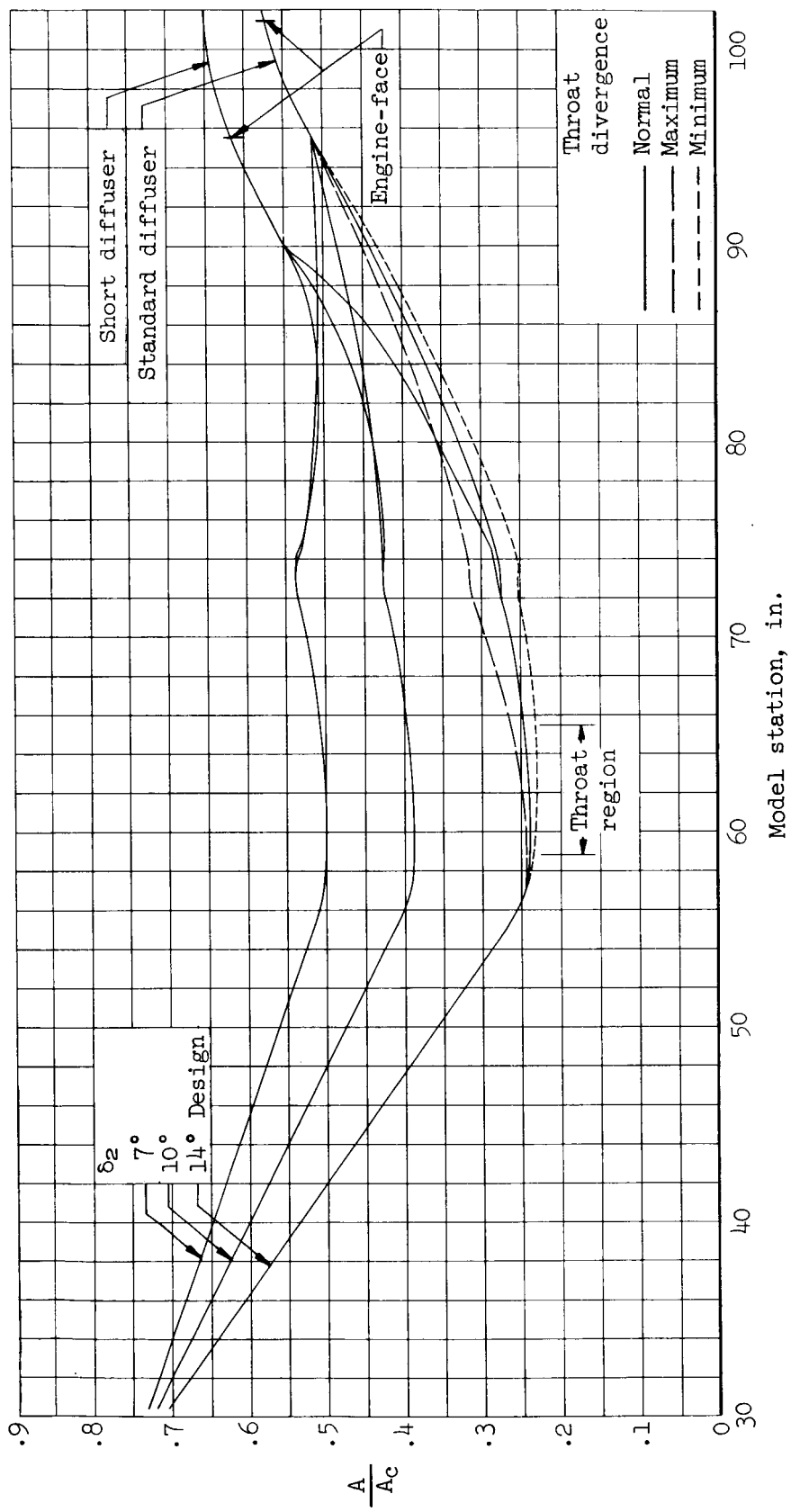
Figure 5.- Variation of diffuser area ratio.
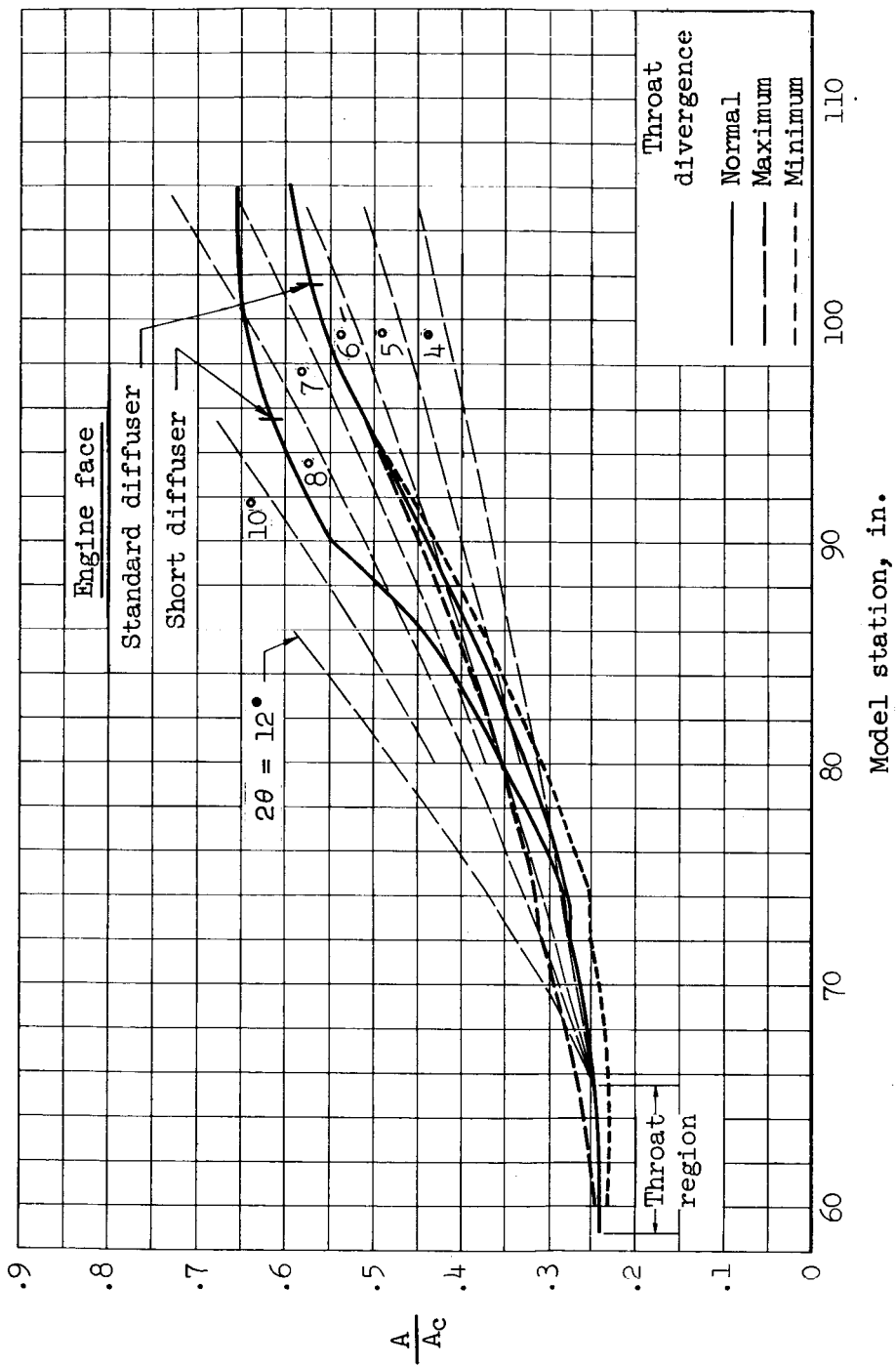
Figure 6.- Variation of subsonic diffuser area ratio; $\delta_2 = 14°$.

23
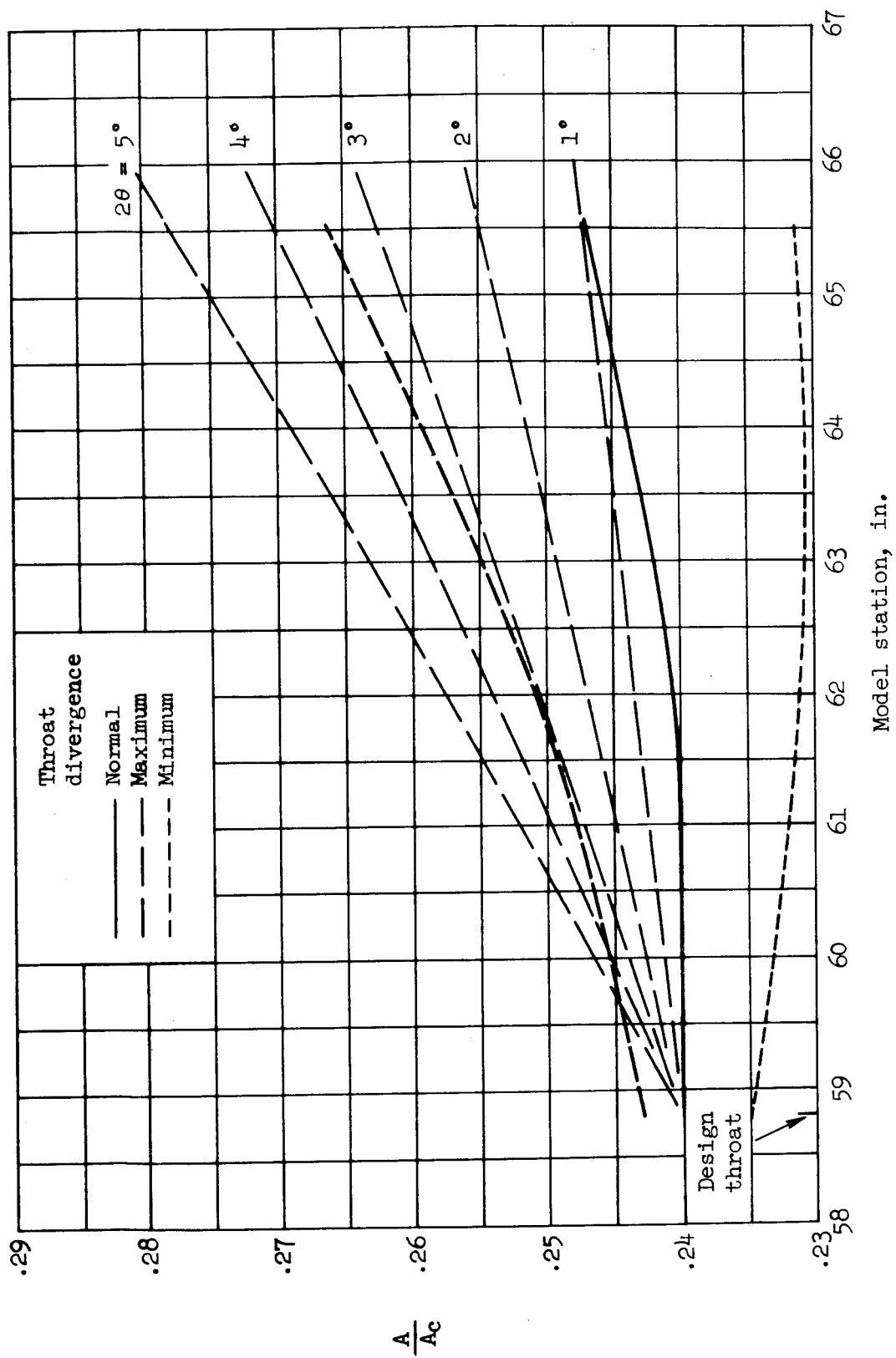
Figure 7.- Variation of throat region area ratio; $\delta_2 = 14°$.

24

(a) Side view.

Figure 8.- Details of model boundary-layer-bleed system, design throat height.
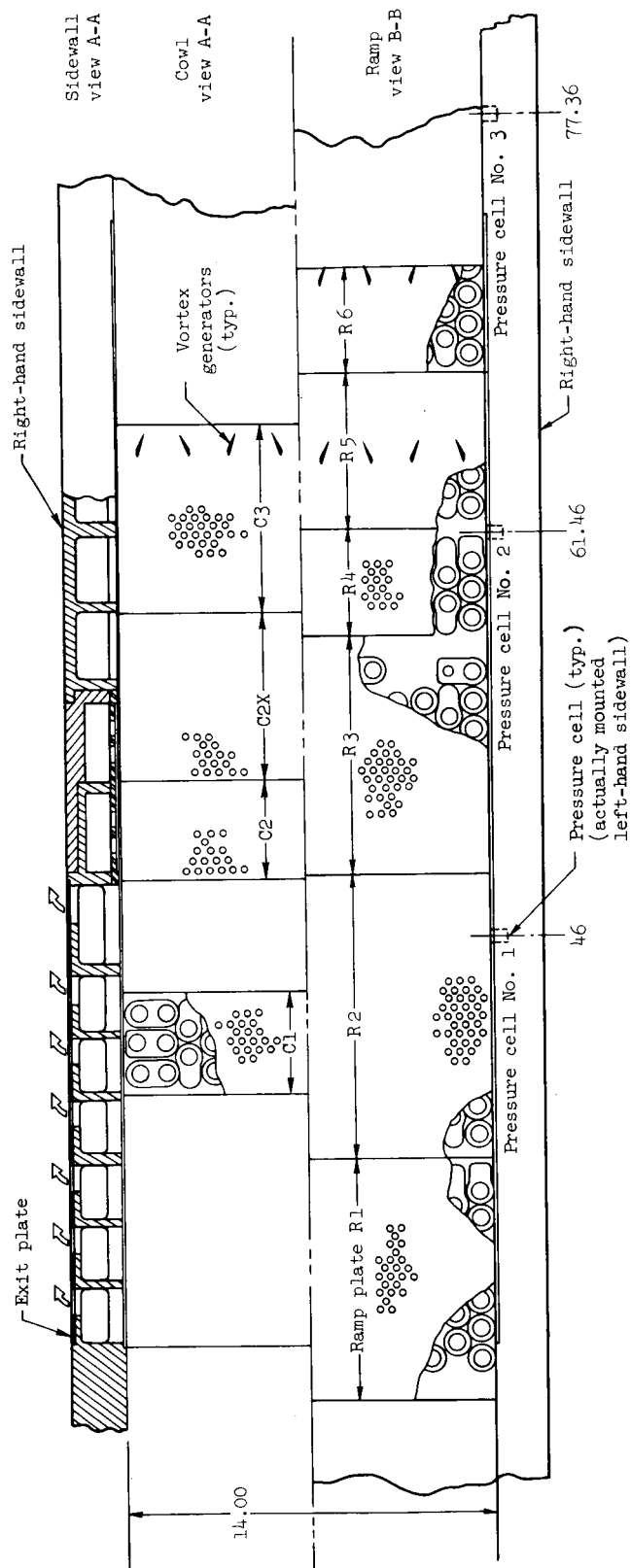
(b) Plan view.

Figure 8.- Continued.

Tangent point

0.09

R = 0.75

0.3

0.502

0.75

0.031 D

1.75

16°

Height
sta.
0

57.08

28.0

$\delta_2 = 14°$

7°

Model sta.
0

14.0

30.4

58.8
Design
throat

64.9

64.5

71.2
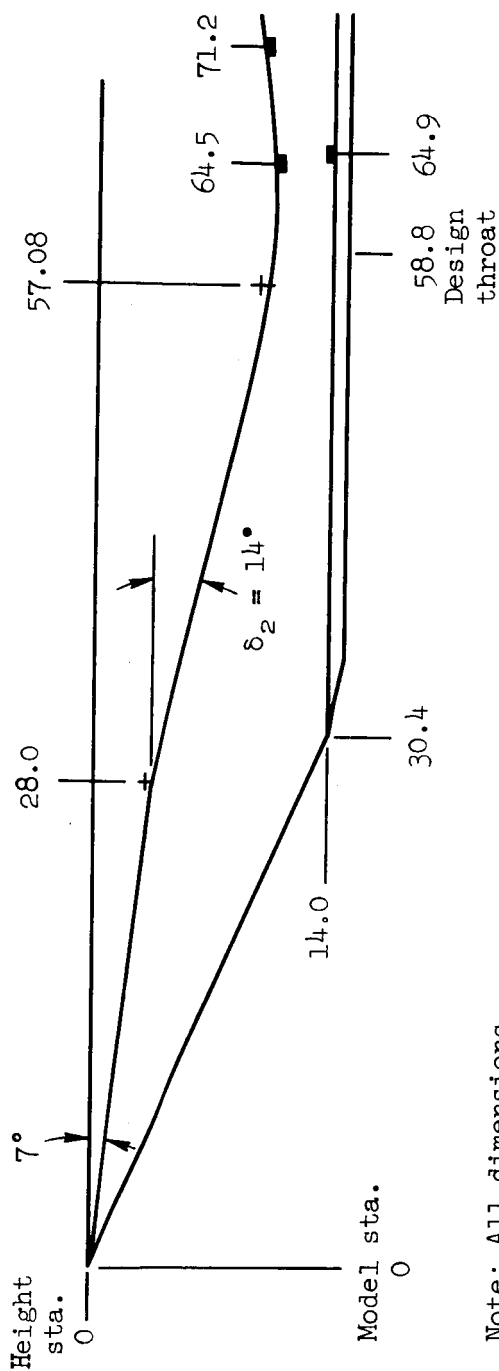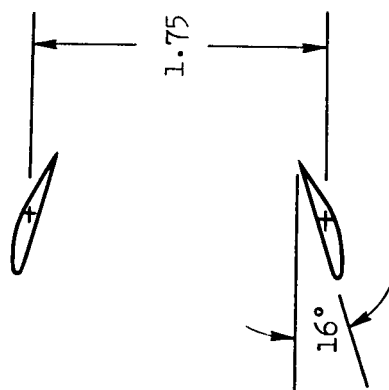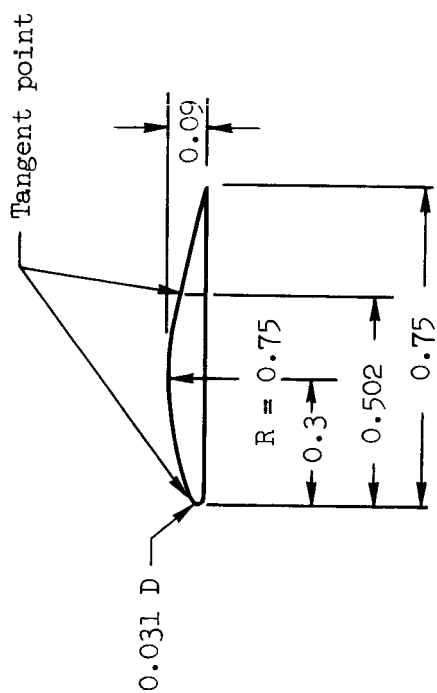
Note: All dimensions
are in inches

(c) Geometry and location of vortex generators.

Figure 8.- Concluded.

27

View looking downstream

● Static pressure
○ Total pressure

DISTANCE FROM WALL			
TUBE NO	A	B OR C	D
1	.13	.26	.13
2	.25	.77	.25
3	.50	1.38	.50
4	.78	2.07	.78
5	1.37	2.89	1.37
6	2.04	3.36	2.04
7	2.85	4.17	2.85
8	3.99	———	3.99
9	———	———	4.67

Note: All dimensions are in inches

Figure 9.- Main duct engine-face instrumentation, standard diffuser.

Figure 10.- Bleed duct pressure instrumentation.
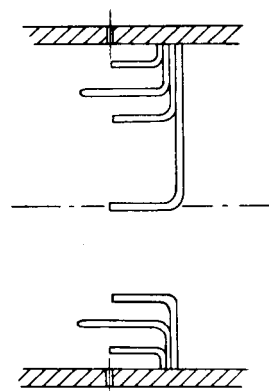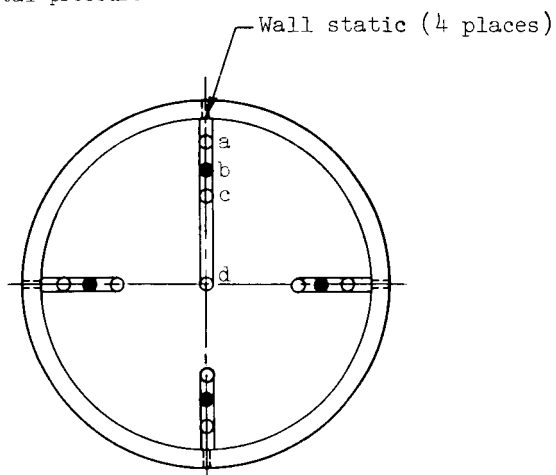
BLEED DUCT	D	L	RAKE TUBE DISTANCE FROM WALL			
			a	b	c	d
1	5.50	11.00	0.350	0.825	1.265	2.750
2	4.25	8.50	0.270	0.638	0.978	2.125
3	5.00	9.00	0.315	0.750	1.100	2.500

$\left(\dfrac{\overline{p}_{t_2}}{p_{t_\infty}}\right)_{max}$

.92

.90

.88

.86

.84

Bleed configuration

◯	24
◻	52
△	54
◇	59
◷	67
◖	77
◈	78
◌	79
◁	80
▽	81
◇	82
◷	83
◖	84
◇	85
◁	86
▷	87

Symbols	Diffuser
Flag up	Short
Flag down	Standard
Open	Standard + VRF
Filled-in	Standard + VRCF

Δp_{t_2} .20   .10   0

.10   .12   .14   .16   .18   .20

$\dfrac{m_{bl}}{m_\infty}$
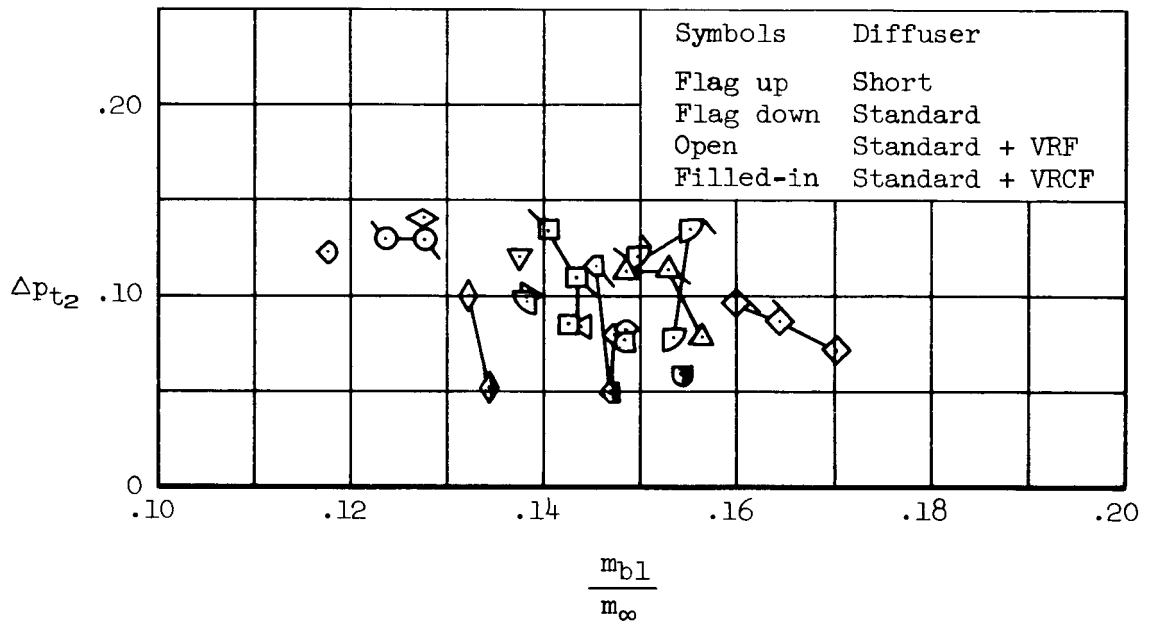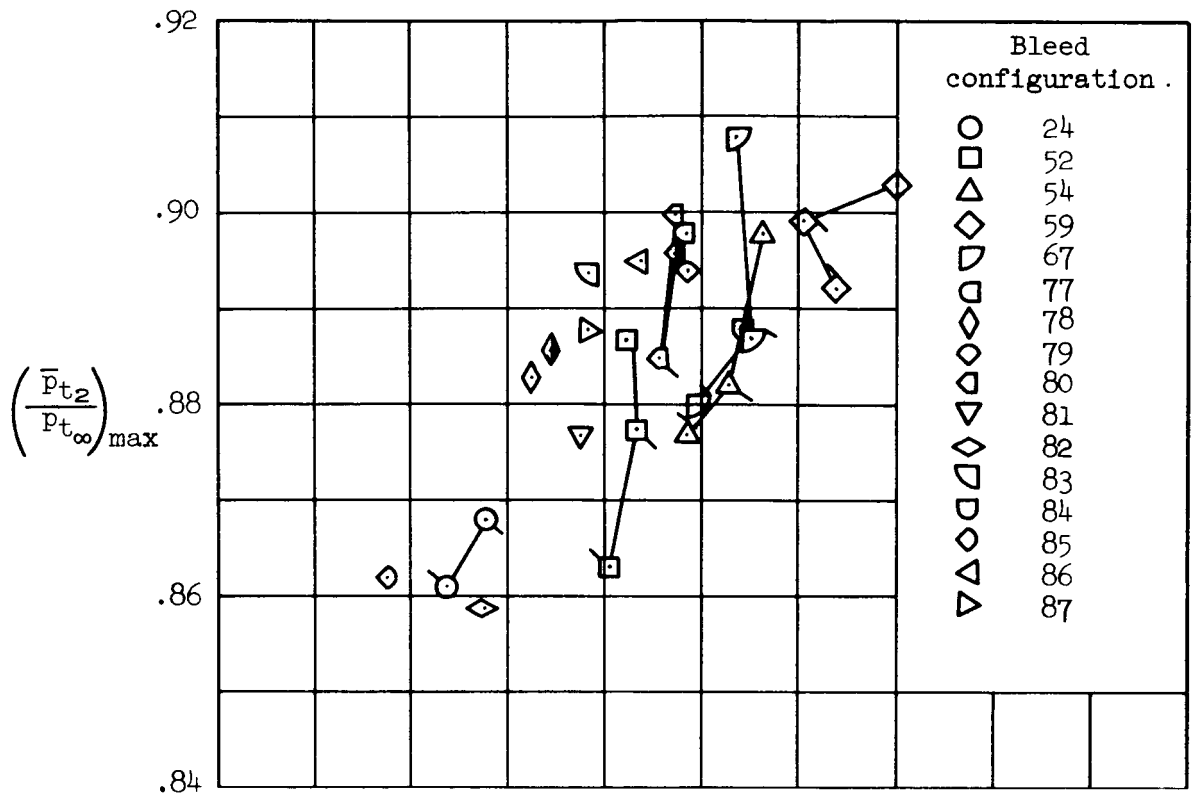
Figure 11.- The effect of boundary-layer-bleed configuration and subsonic diffuser design on engine-face maximum recovery performance; optimum divergence, $M_\infty = 3.0$, $\alpha = 0°$.
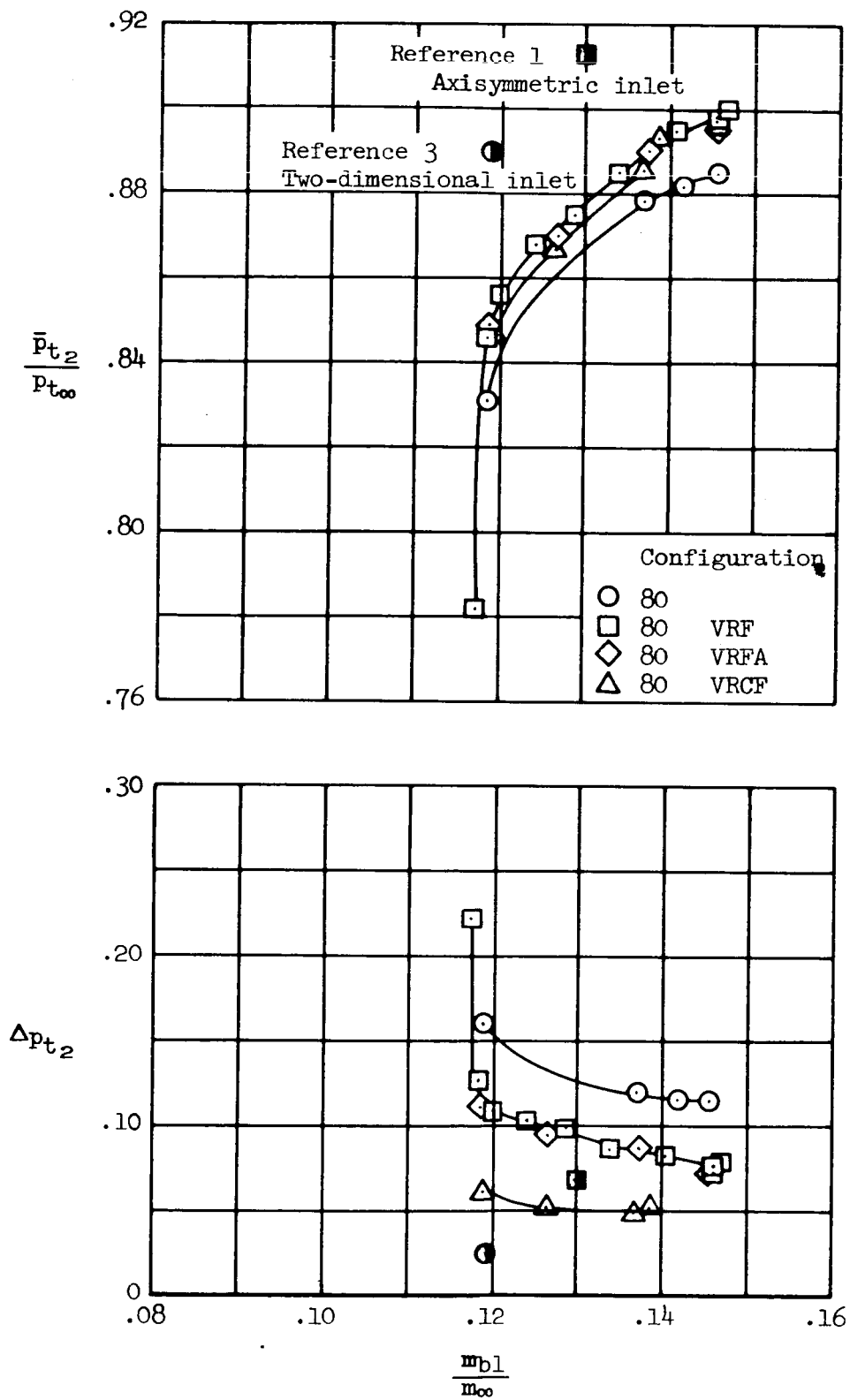
Figure 12.- The effect of vortex generators on engine-face total-pressure performance; bleed configuration 80, $M_\infty = 3.0$, $\alpha = 0°$.
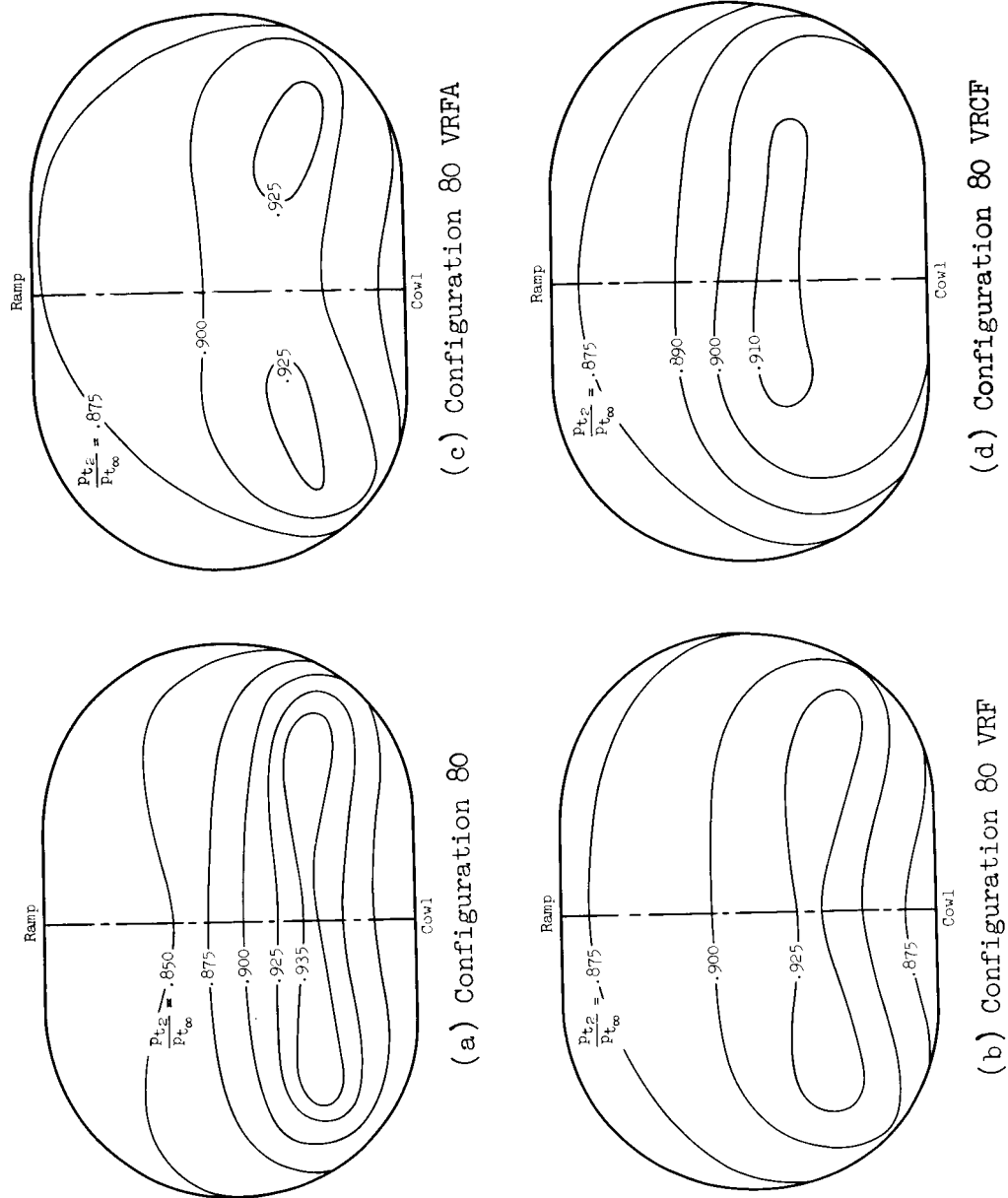
Figure 13.- The effect of vortex generators on engine-face total-pressure contours for maximum total-pressure recovery; bleed configuration 80, $M_\infty = 3.0$, $\alpha = 0°$.

(a) Configuration 80

(b) Configuration 80 VRF

(c) Configuration 80 VRFA

(d) Configuration 80 VRCF

32
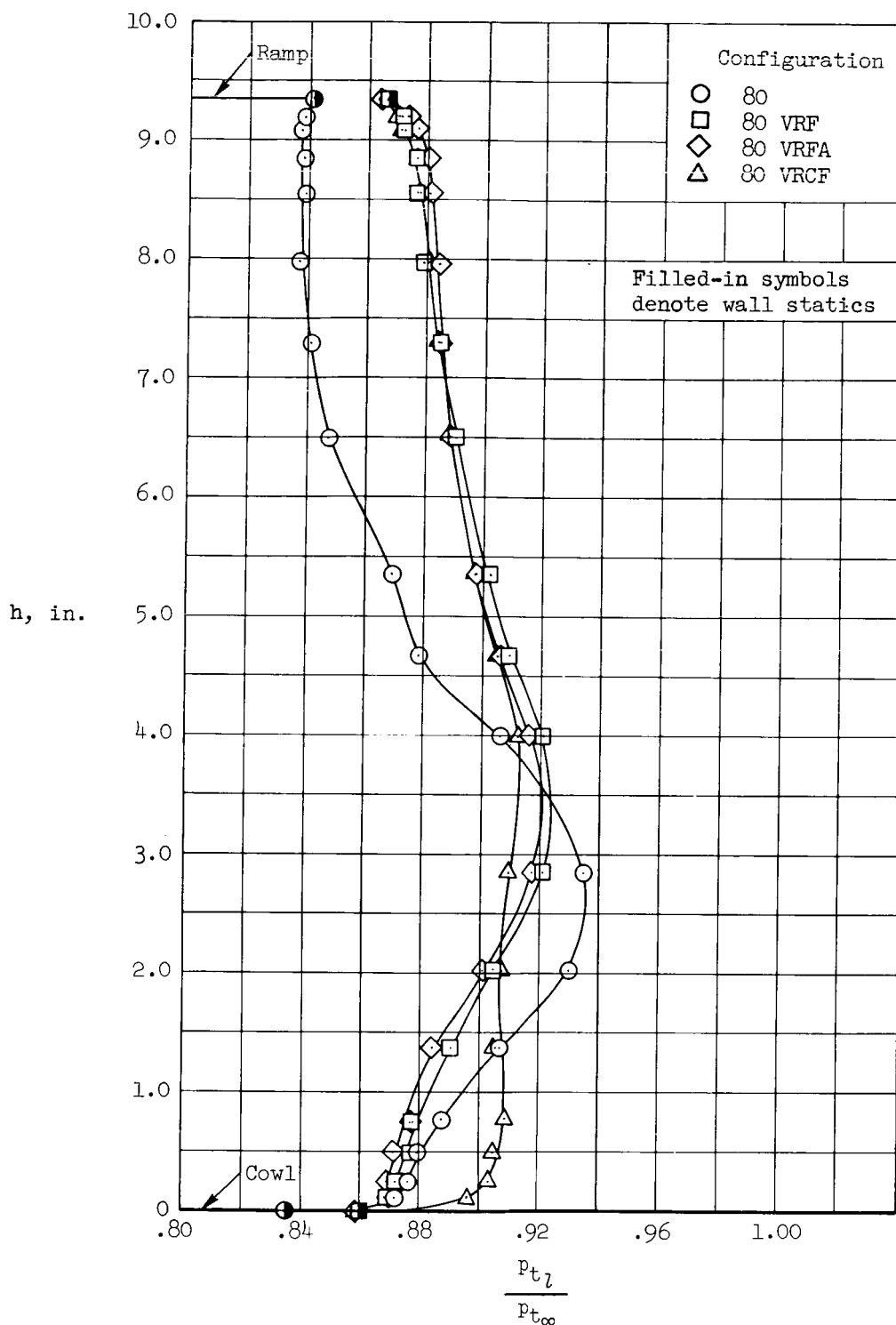
Figure 14.- The effect of vortex generators on engine-face vertical total-pressure profiles for maximum total-pressure recovery; bleed configuration 80, $M_\infty = 3.0$, $\alpha = 0°$.
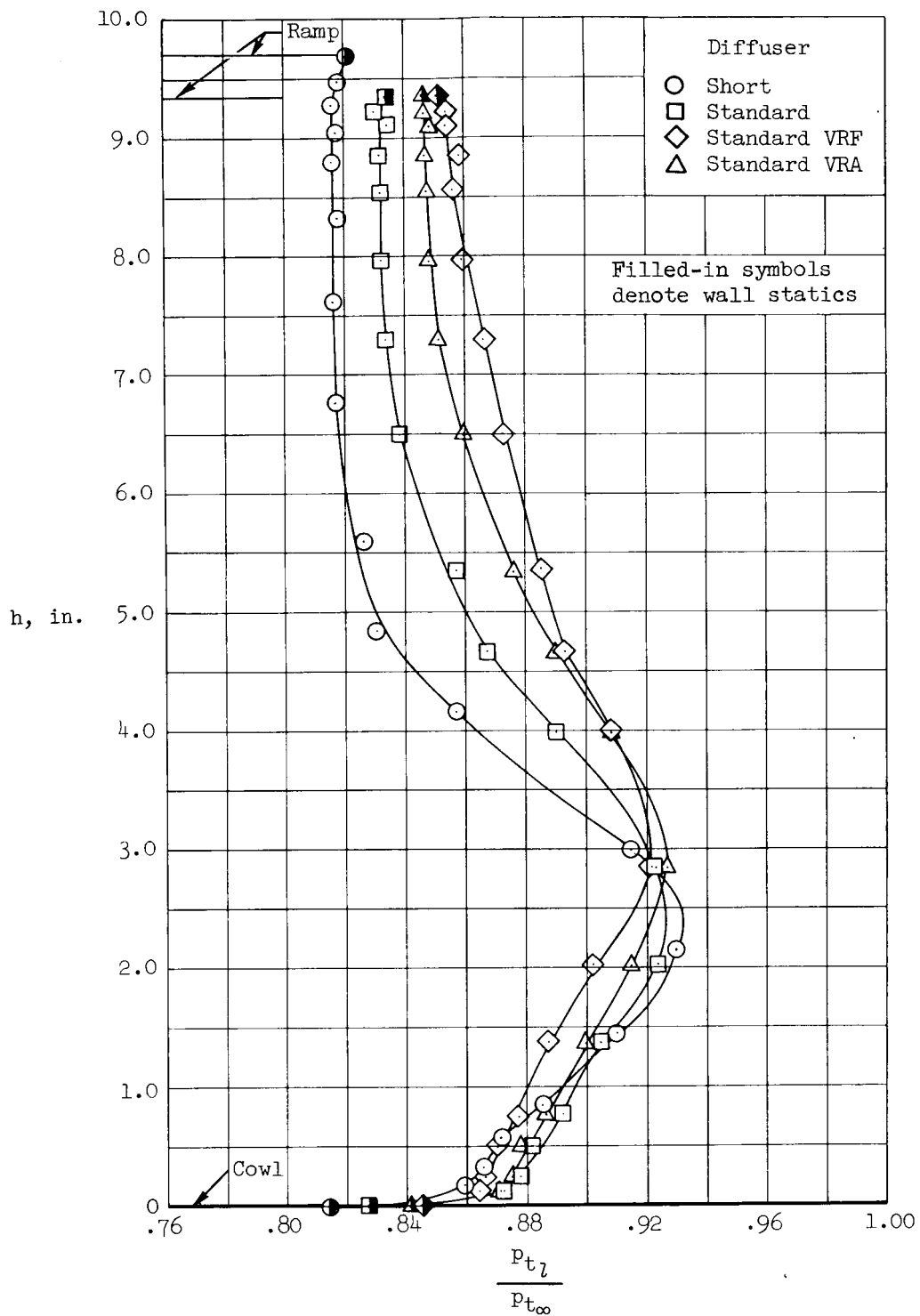
(a) Bleed configuration 52.

Figure 15.- The effect of subsonic diffuser design and vortex generators on engine-face vertical total-pressure profiles for maximum total-pressure recovery; optimum divergence, M_∞ = 3.0, α = 0°.
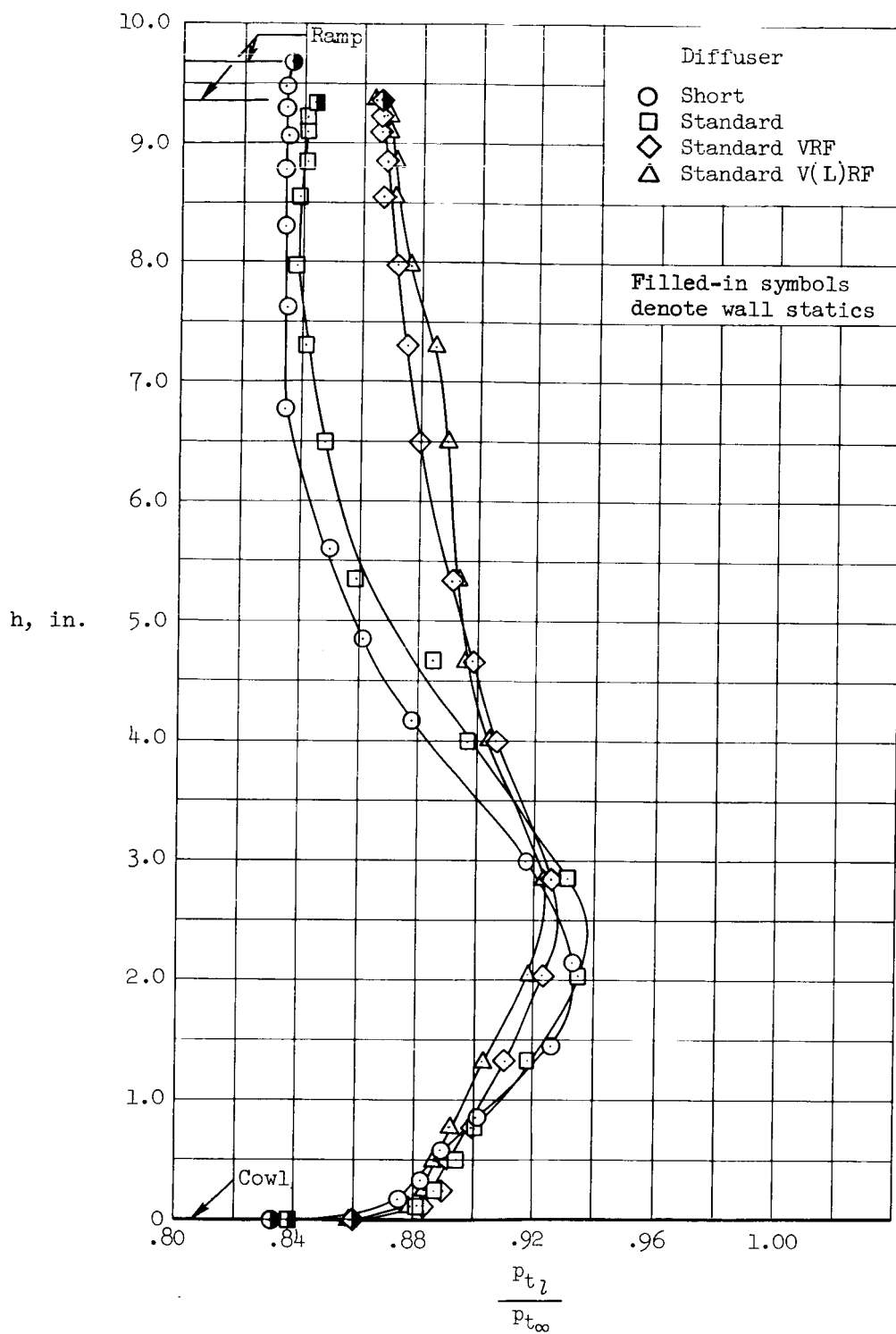
(b) Bleed configuration 54.

Figure 15.- Continued.
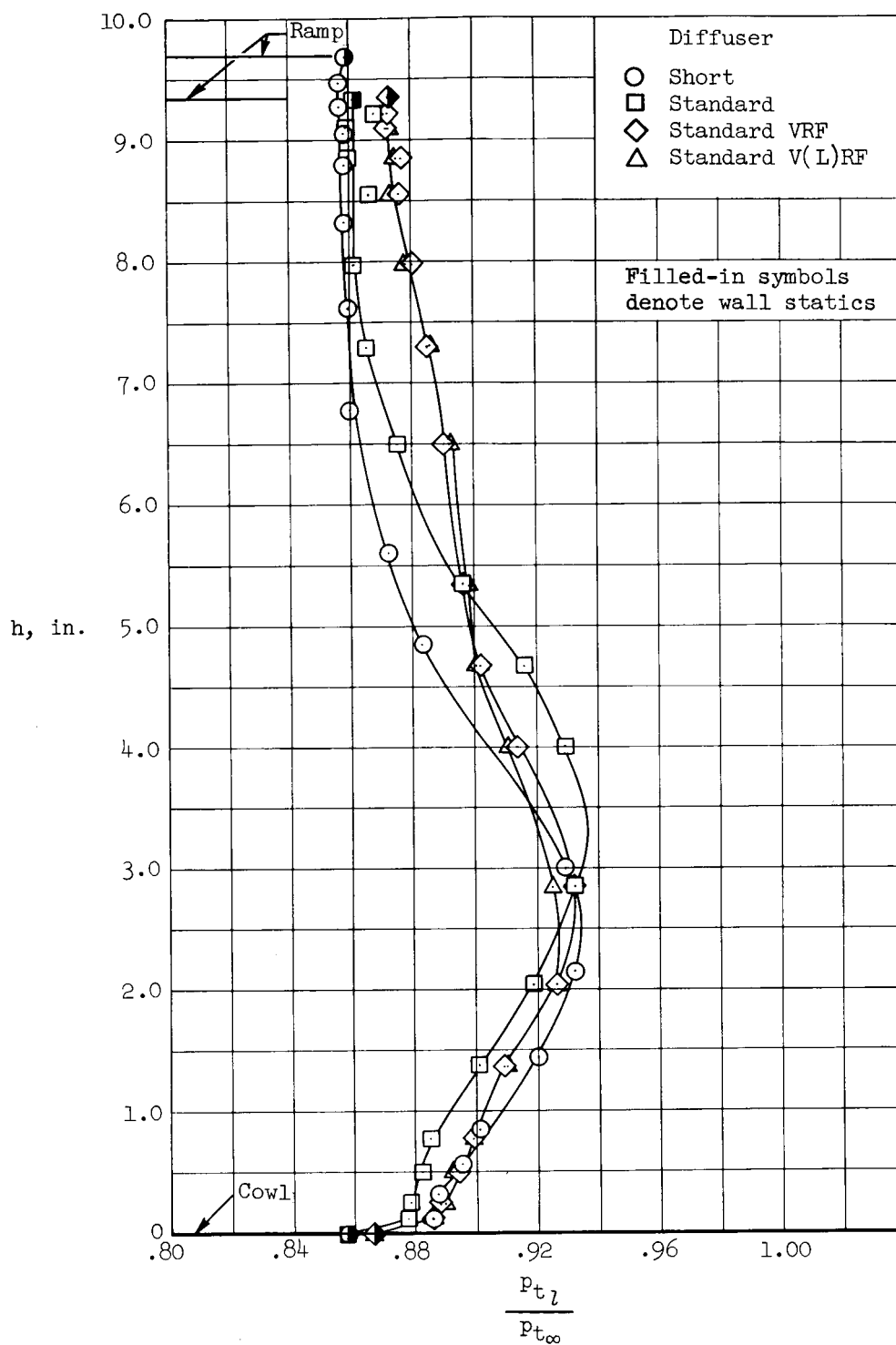
(c) Bleed configuration 59.

Figure 15.- Continued.
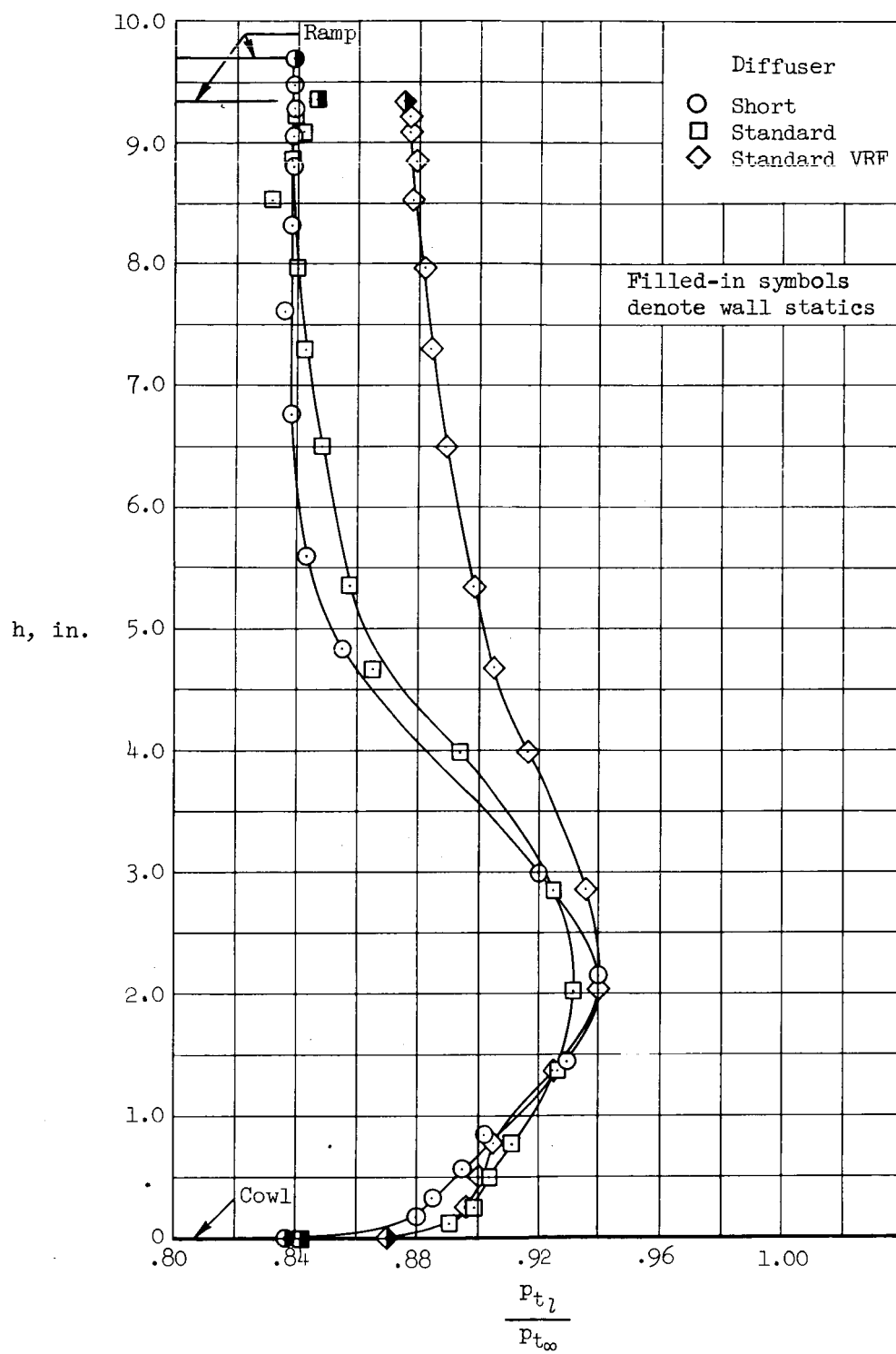
(d) Bleed configuration 67.

Figure 15.- Concluded.
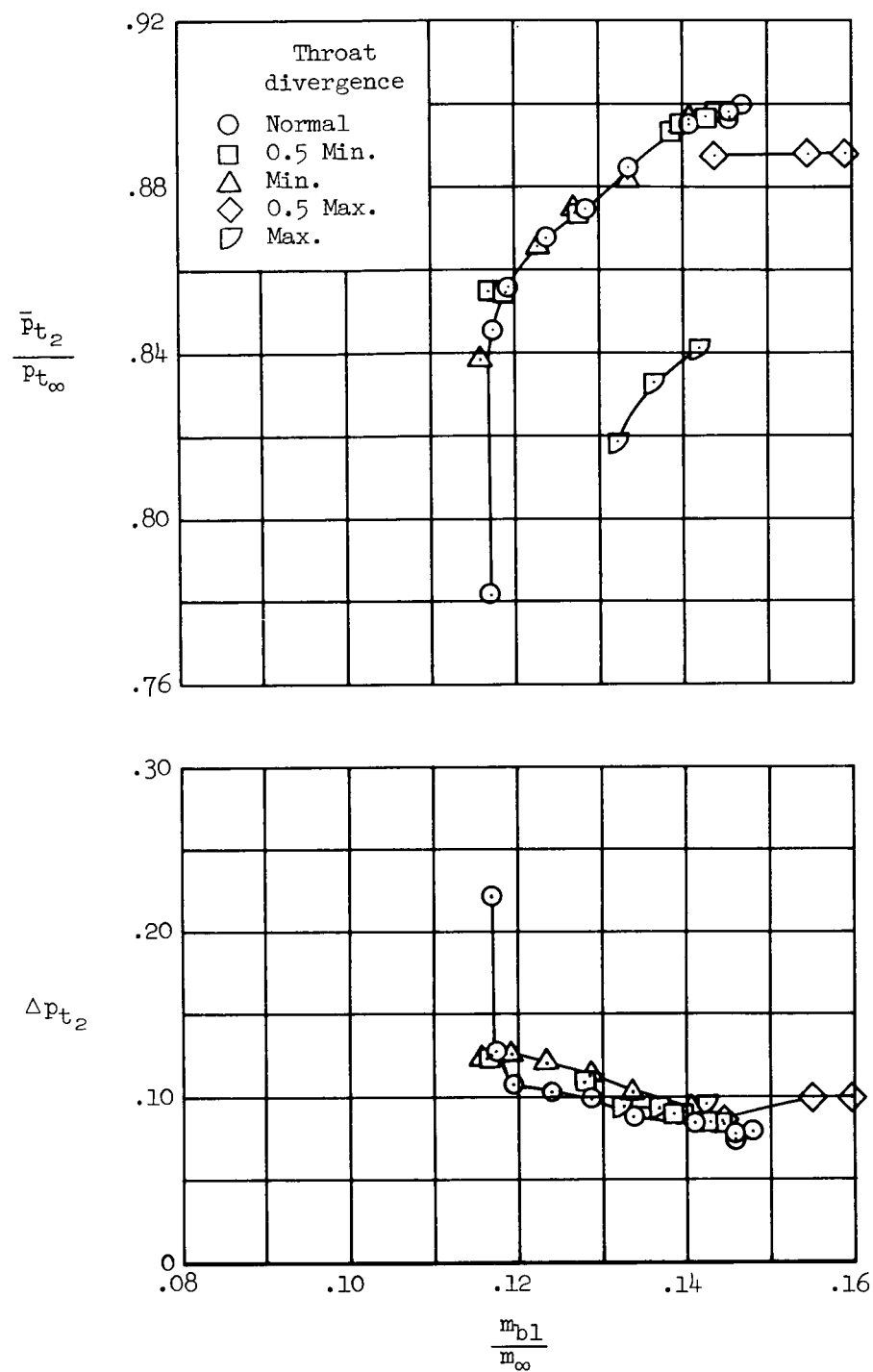
Figure 16.- The effect of throat divergence on engine-face total-pressure performance; configuration 80 VRF, $M_\infty = 3.0$, $\alpha = 0°$.
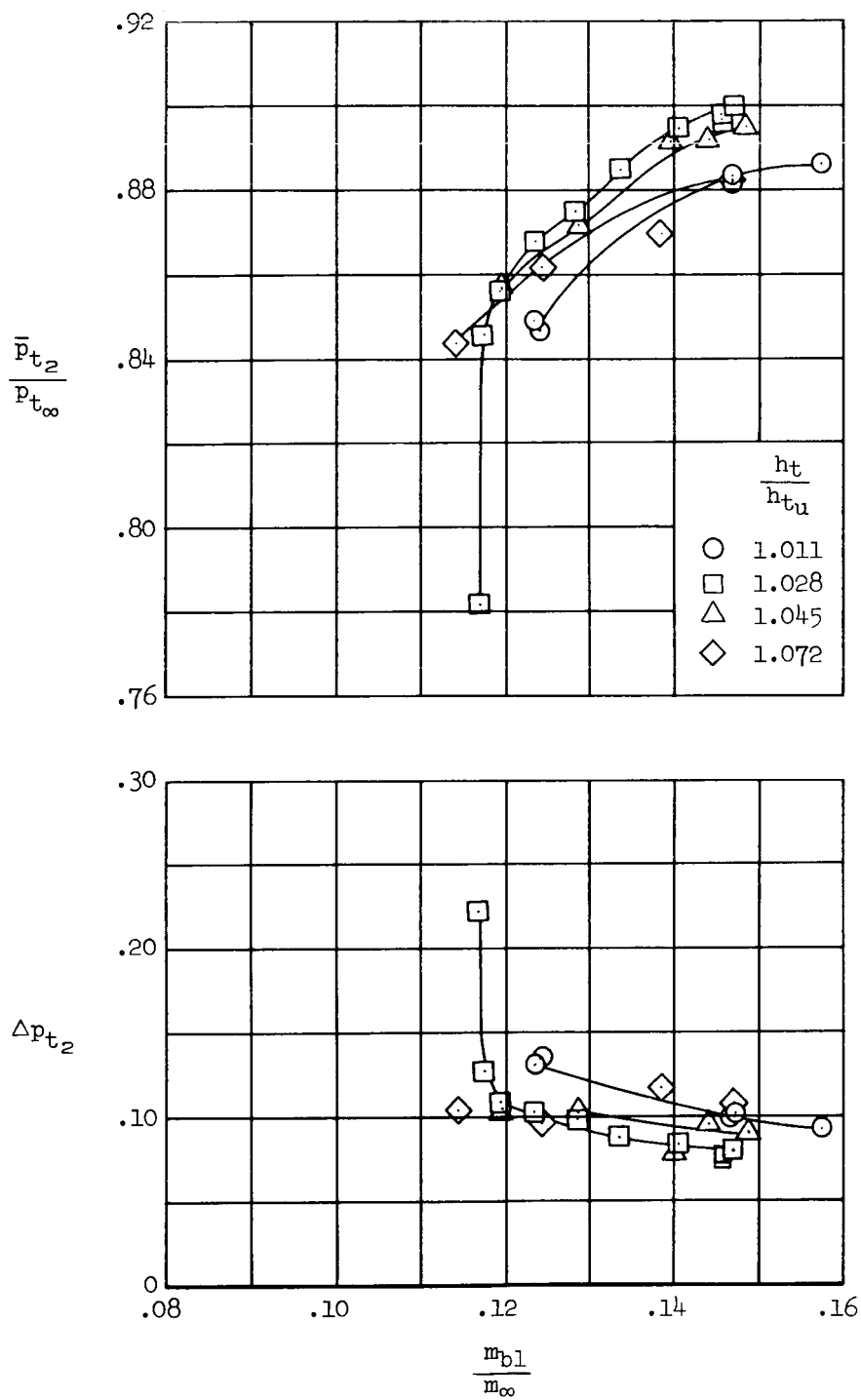
Figure 17.- The effect of throat height on engine-face total-pressure
performance; configuration 80 VRF, $M_\infty = 3.0$, $\alpha = 0°$.
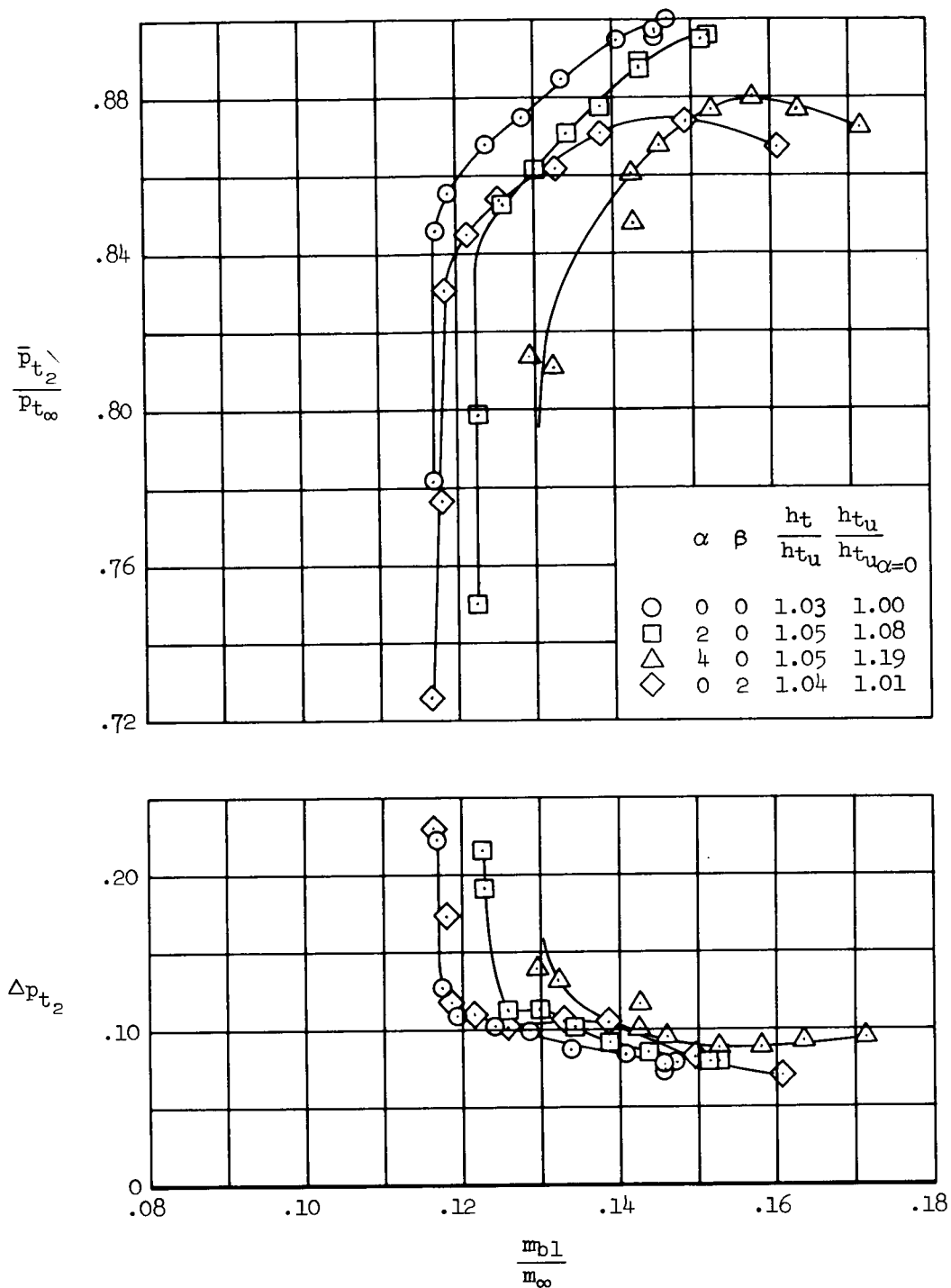
(a) Boundary-layer-bleed mass-flow ratio.

Figure 18.- The effect of angle of attack and yaw on engine-face total-pressure performance; configuration 80 VRF, $M_\infty = 3.0$, $\alpha = 0°$.
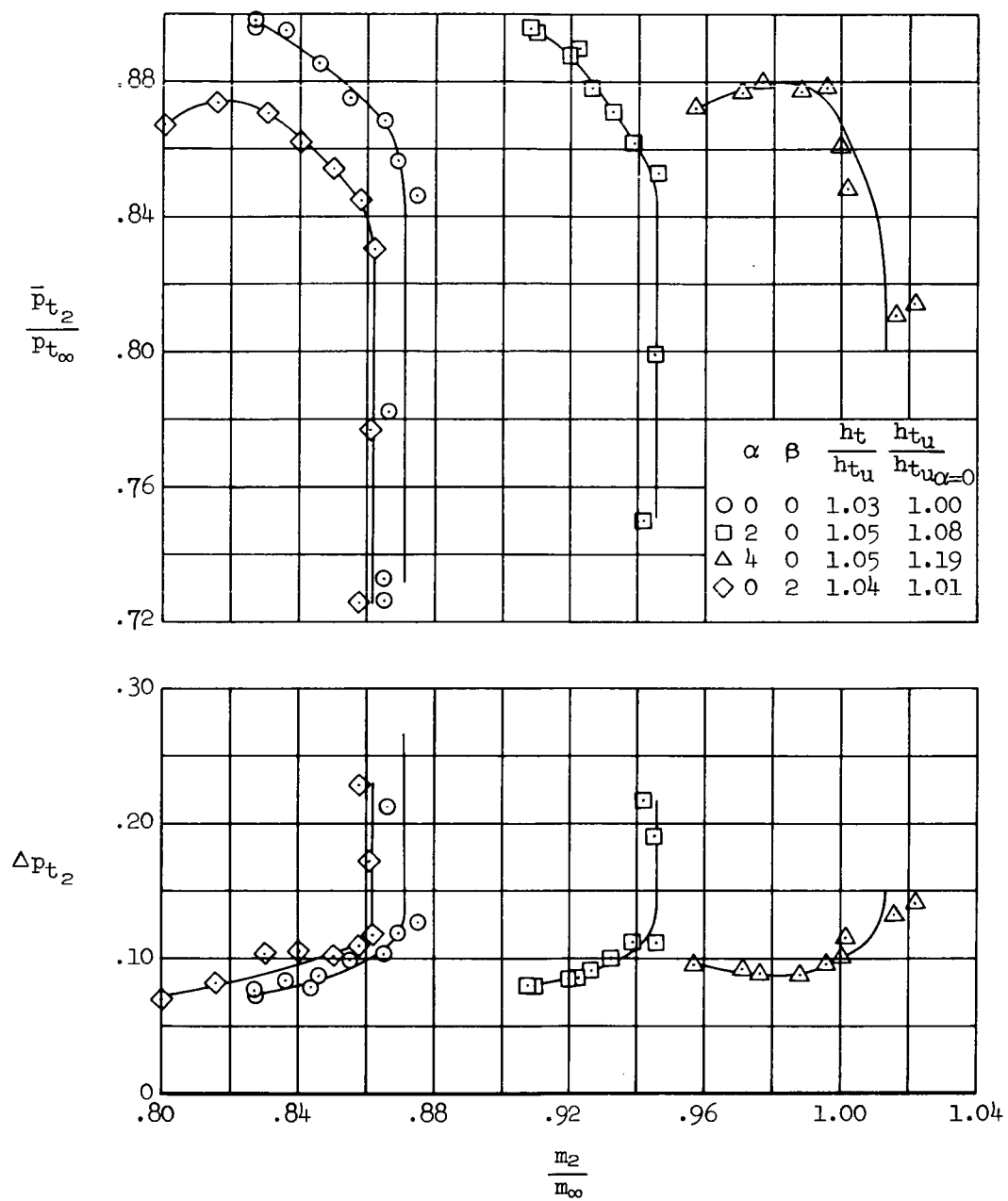
(b) Main duct mass-flow ratio.

Figure 18.- Concluded.
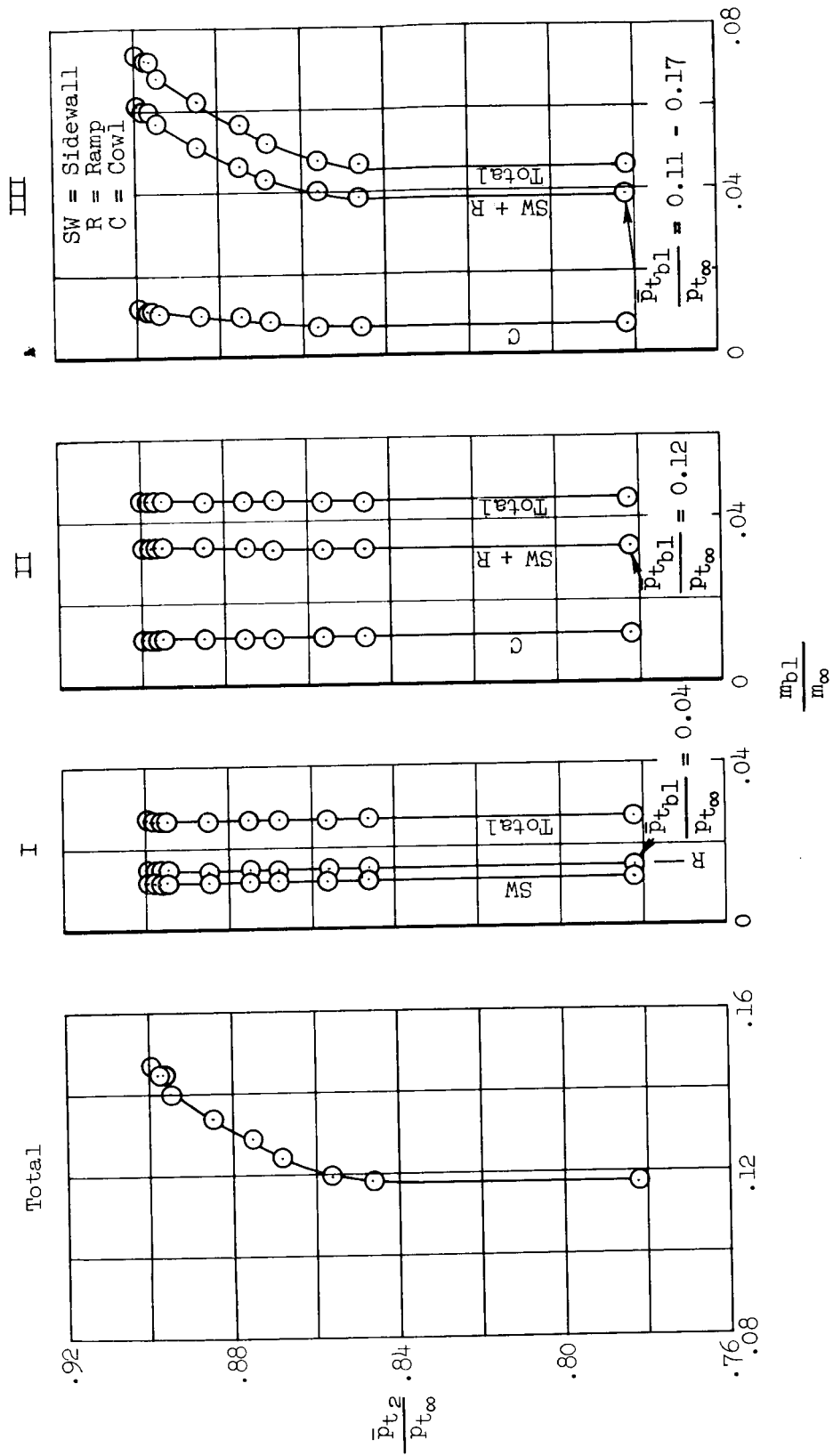
Figure 19.- Boundary-layer-bleed performance; reference configuration 80 VRF, $M_\infty = 3.0$, $\alpha = 0°$.
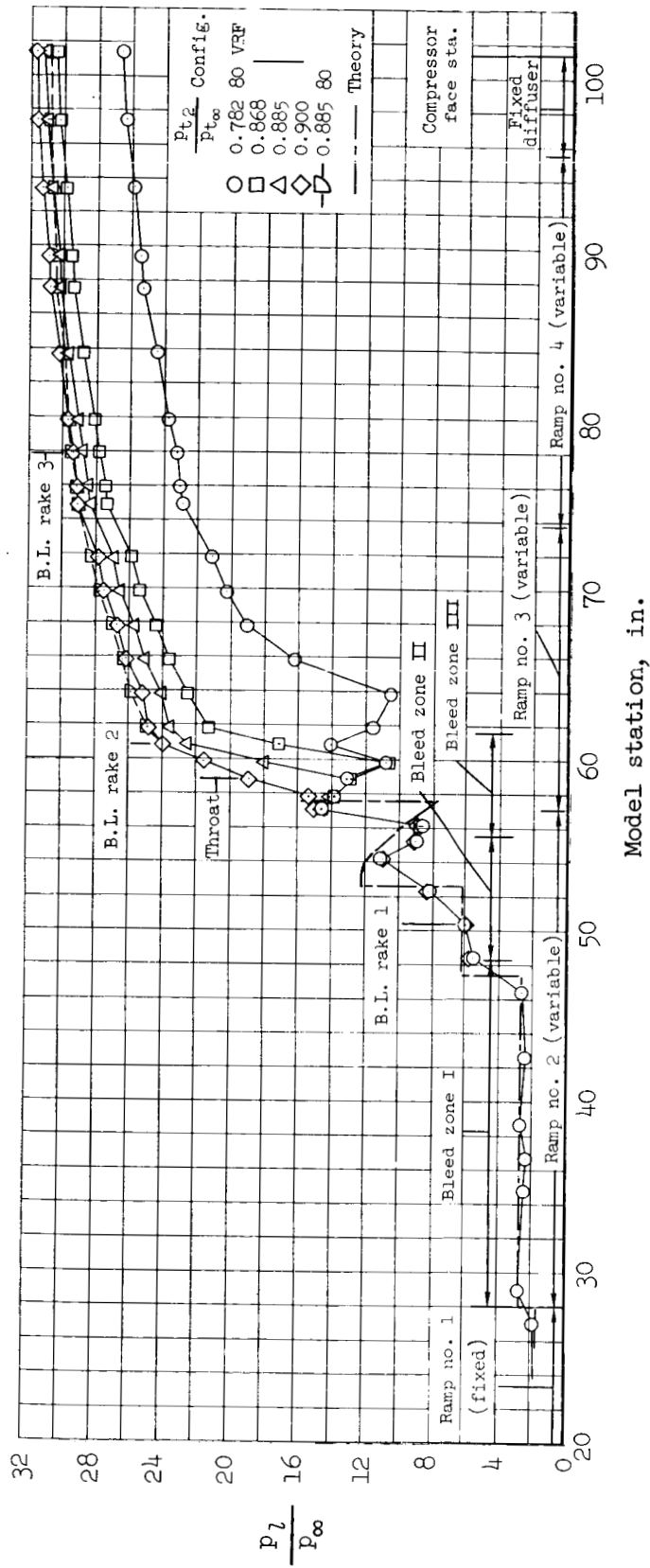
Figure 20.- Static-pressure ratio distribution; configurations 80 and 80 VRF, $M_\infty = 3.0$, $\alpha = 0°$.

(a) Ramp.

43
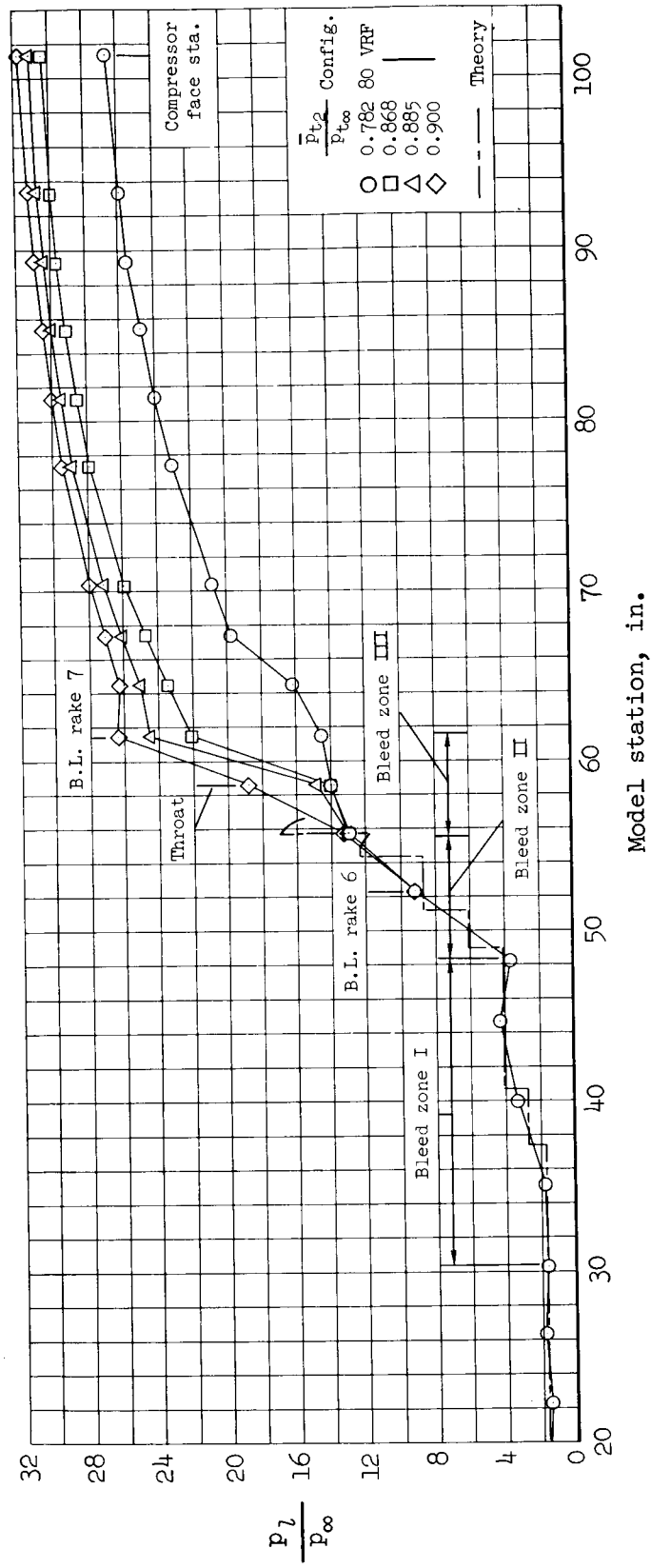
(b) Sidewall.

Figure 20.- Continued.
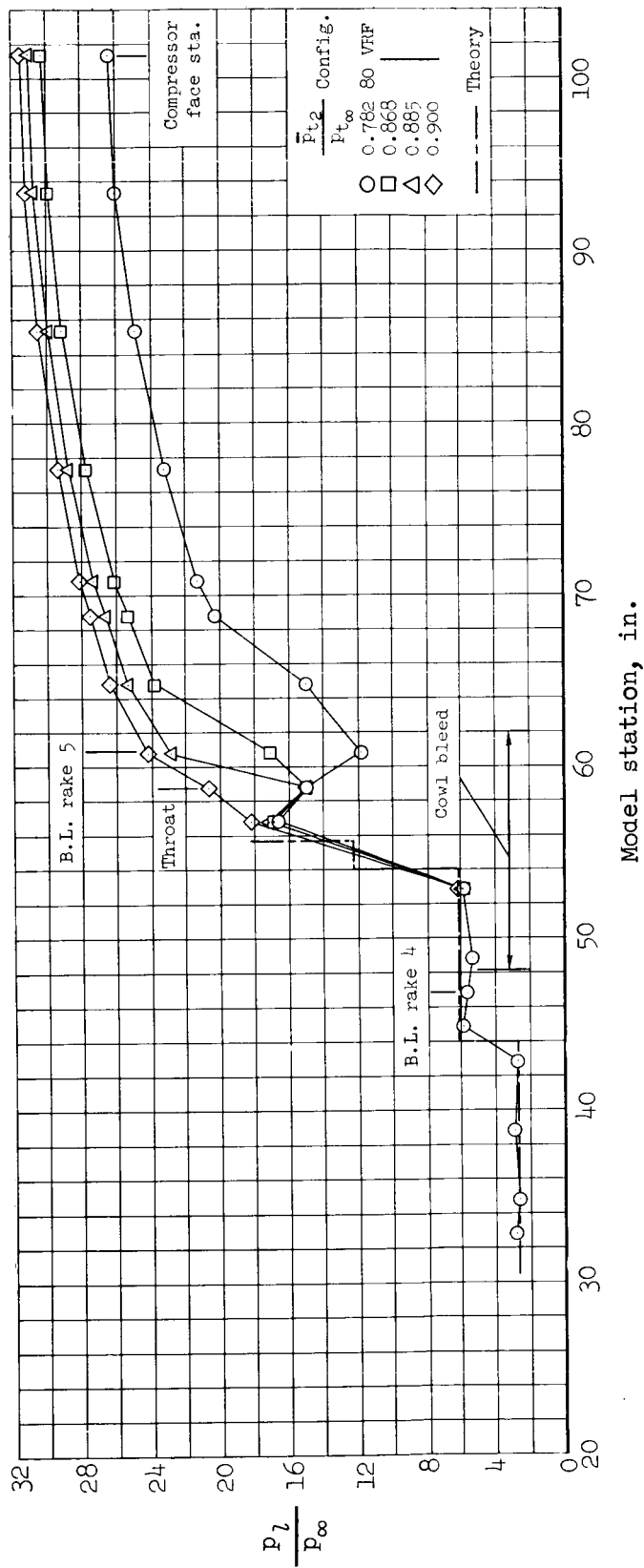
(c) Cowl.

Figure 20.- Concluded.
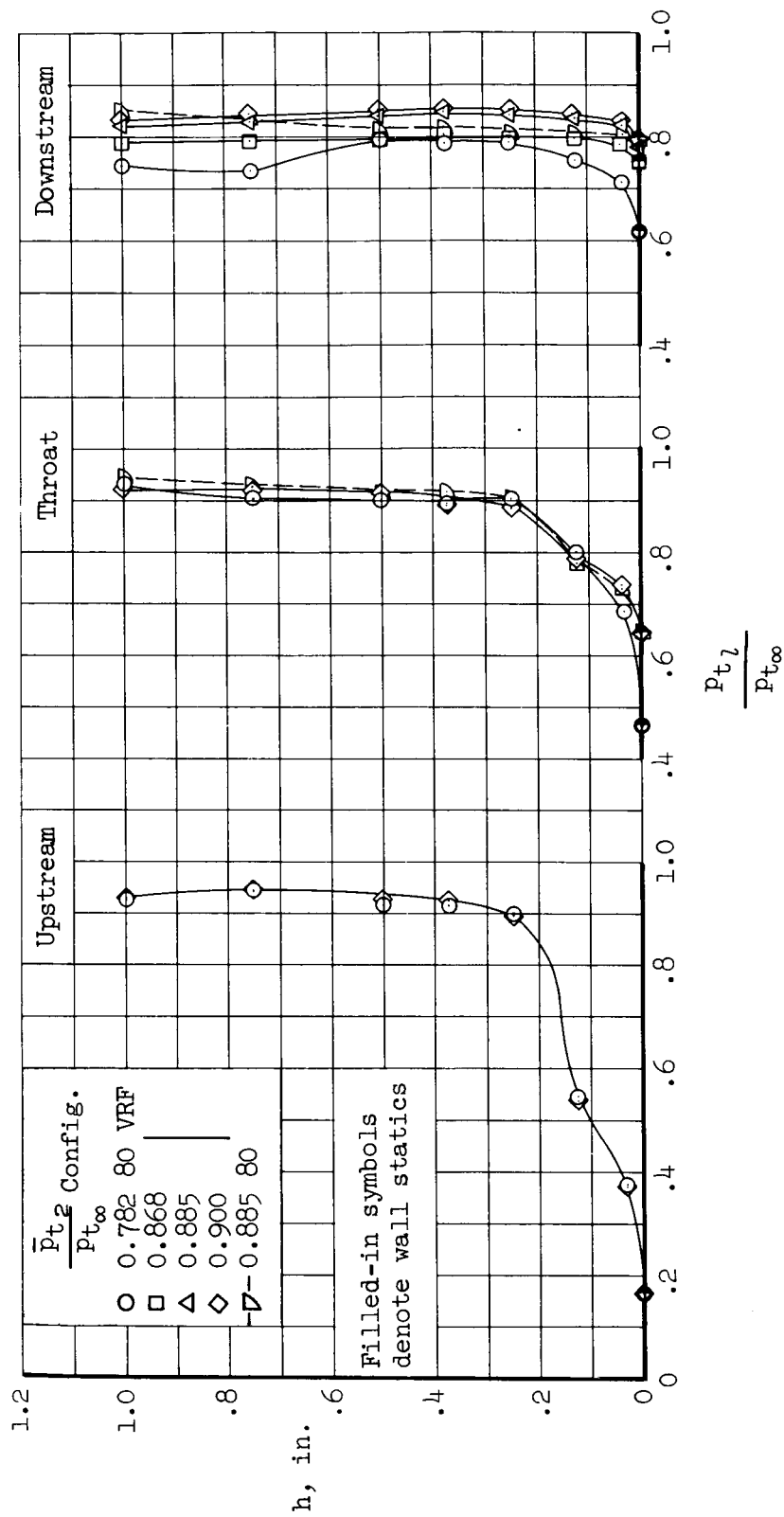
(a) p_{t_l}/p_{t_∞}

Figure 21.- Ramp boundary-layer characteristics; configurations 80 and 80 VRF, $M_\infty = 3.0$, $\alpha = 0°$.
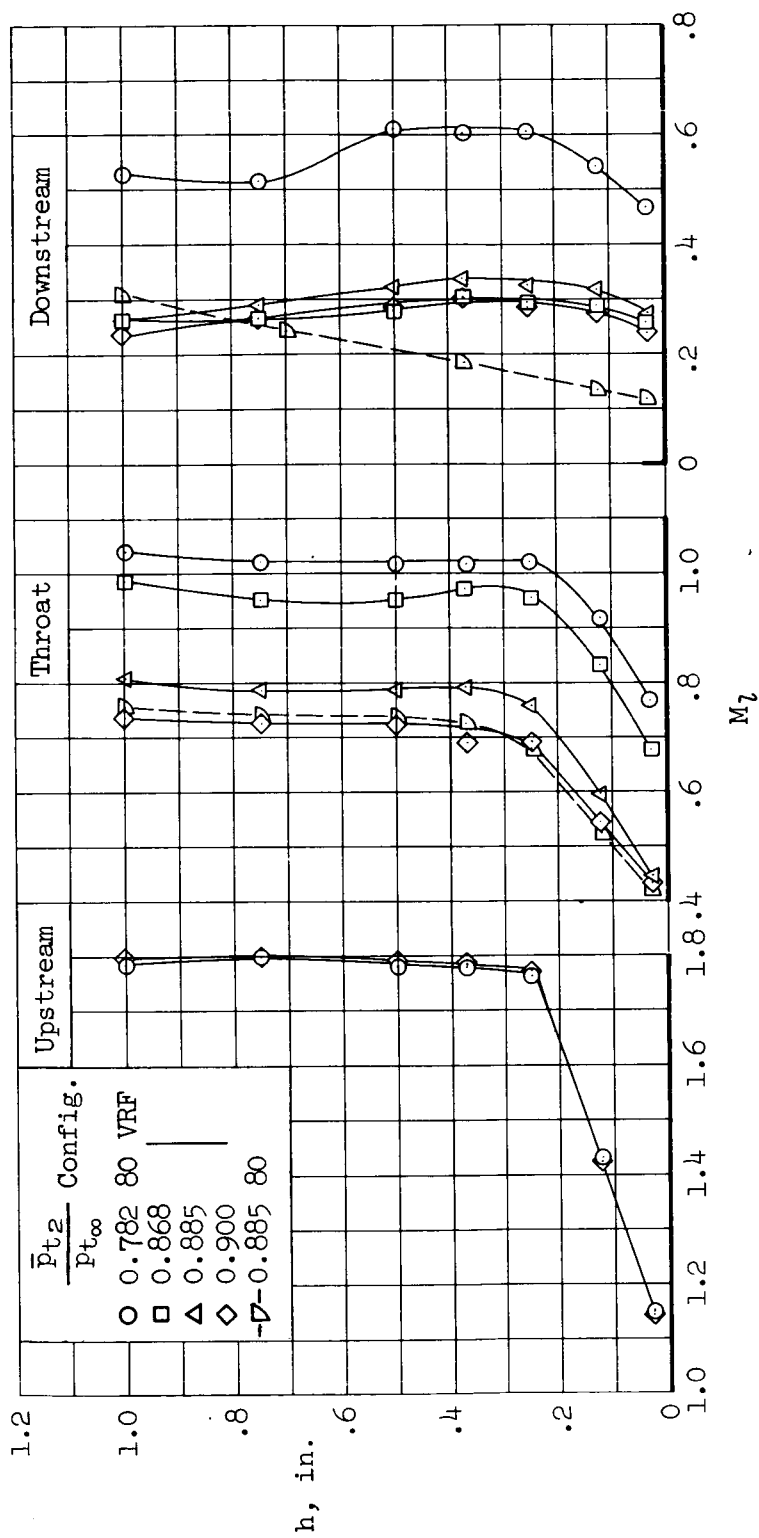
(b) M_l

Figure 21.- Continued.

(c) V_l/V_o
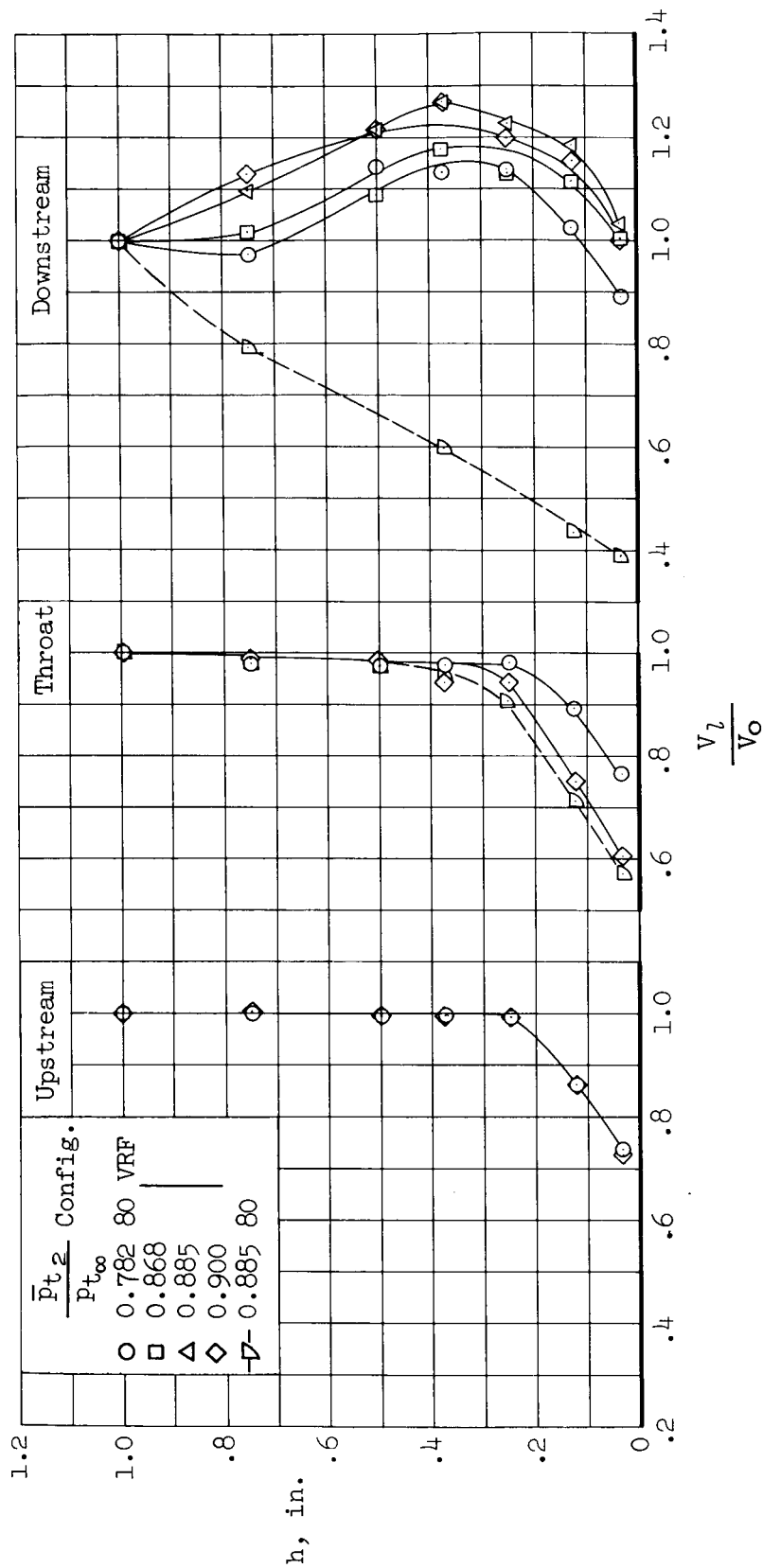
Figure 21.- Concluded.
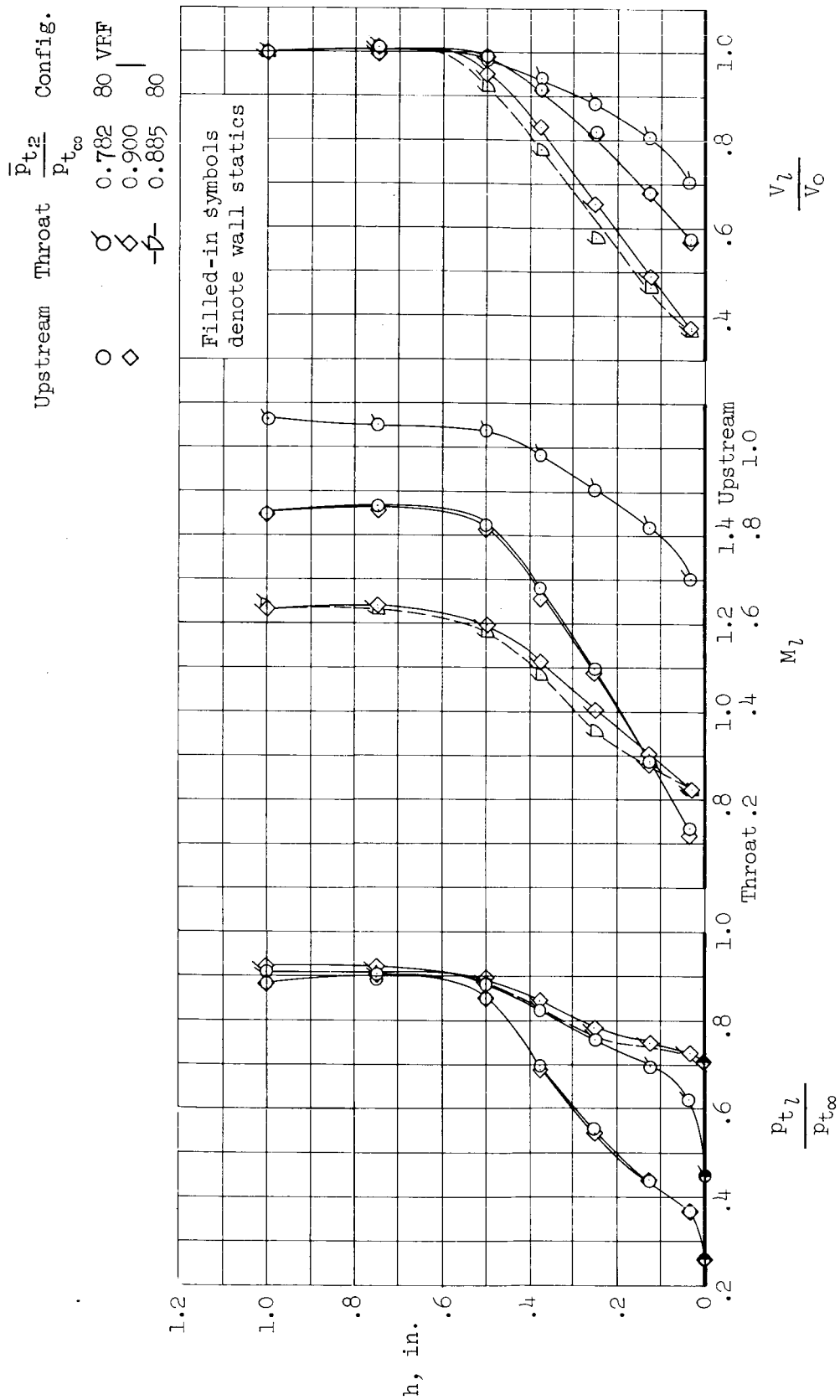
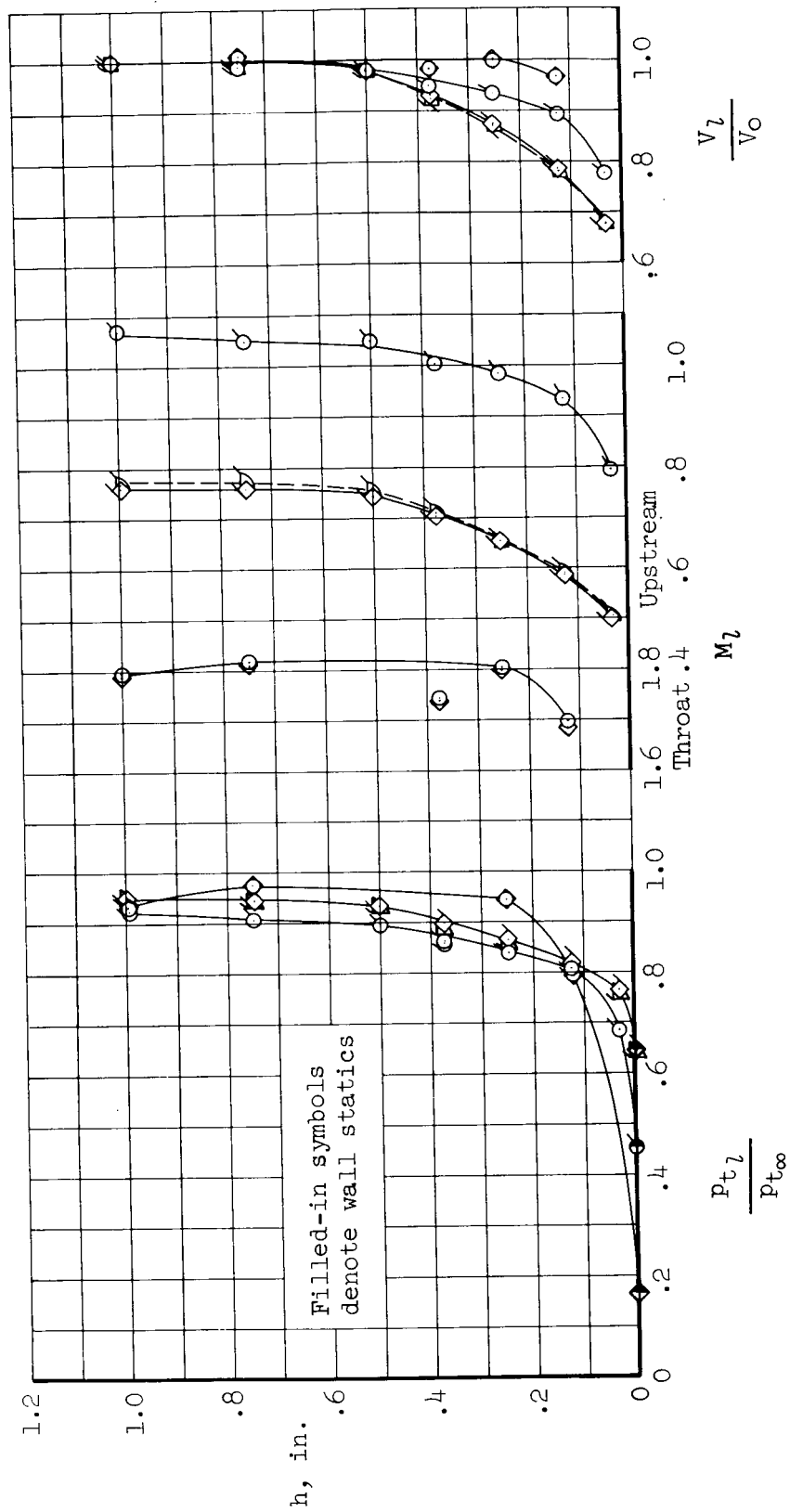Figure 22.- Sidewall boundary-layer characteristics; configurations 80 and 80 VRF, $M_\infty = 3.0$, $\alpha = 0°$.

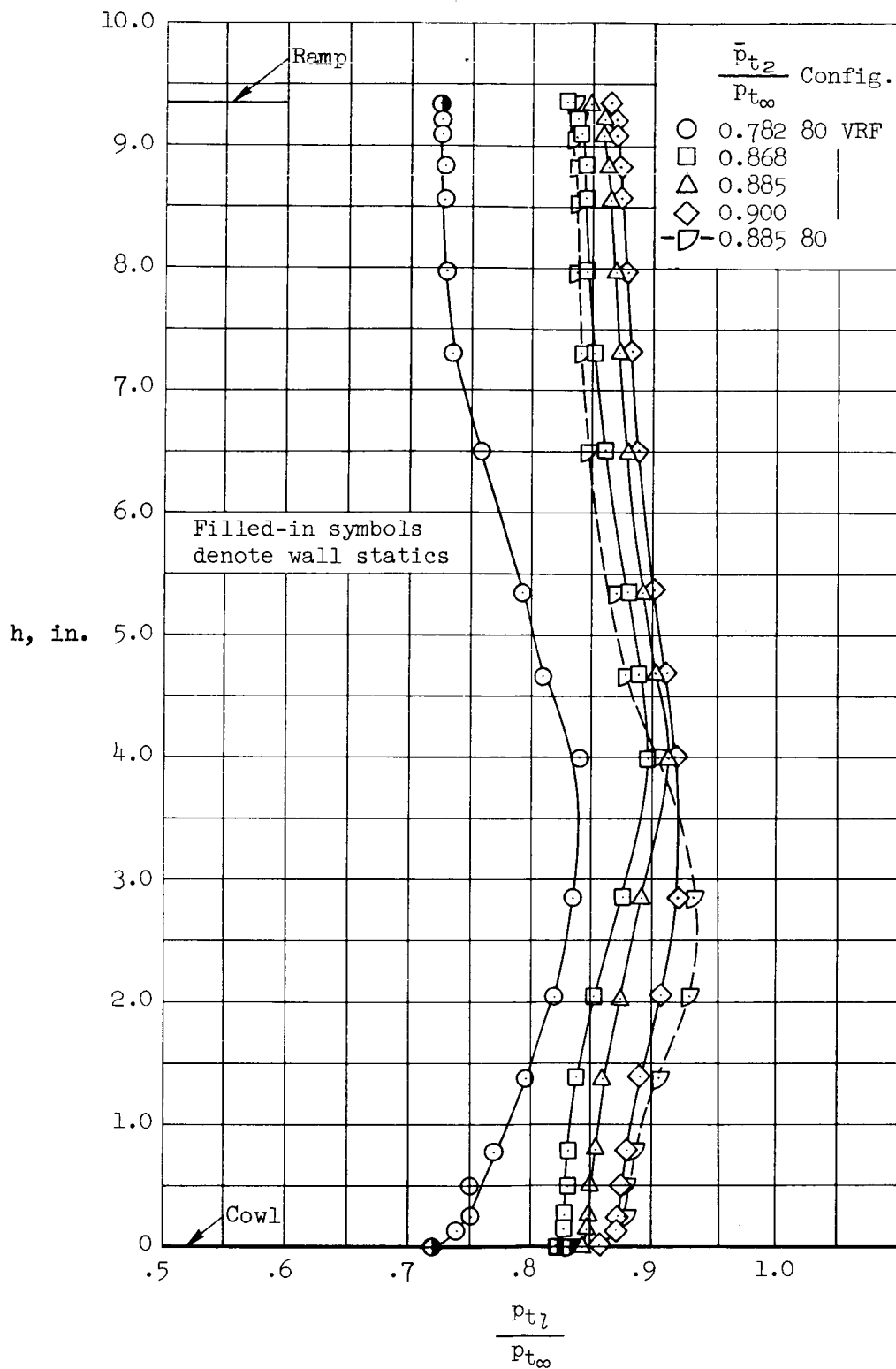Figure 23.- Cowl boundary-layer characteristics; configurations 80 and 80 VRF, $M_\infty = 3.0$, $\alpha = 0°$.

Figure 24.- Engine-face vertical total-pressure profiles; configurations 80 VRF and 80, $M_\infty = 3.0$, $\alpha = 0°$.
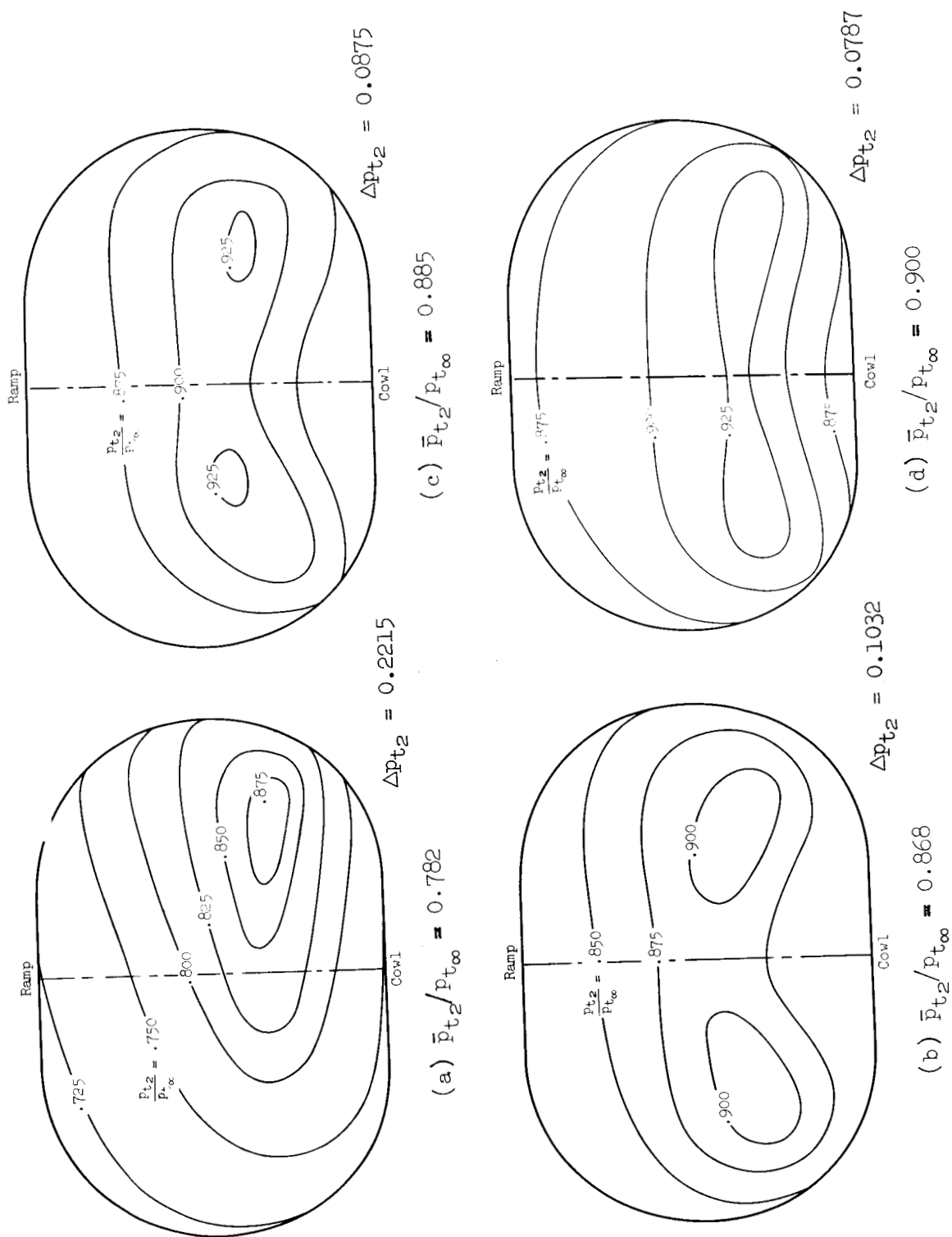
$\Delta p_{t_2} = 0.2215$

(a) $\bar{p}_{t_2}/p_{t_\infty} = 0.782$

$\Delta p_{t_2} = 0.0875$

(c) $\bar{p}_{t_2}/p_{t_\infty} = 0.885$

$\Delta p_{t_2} = 0.1032$

(b) $\bar{p}_{t_2}/p_{t_\infty} = 0.868$

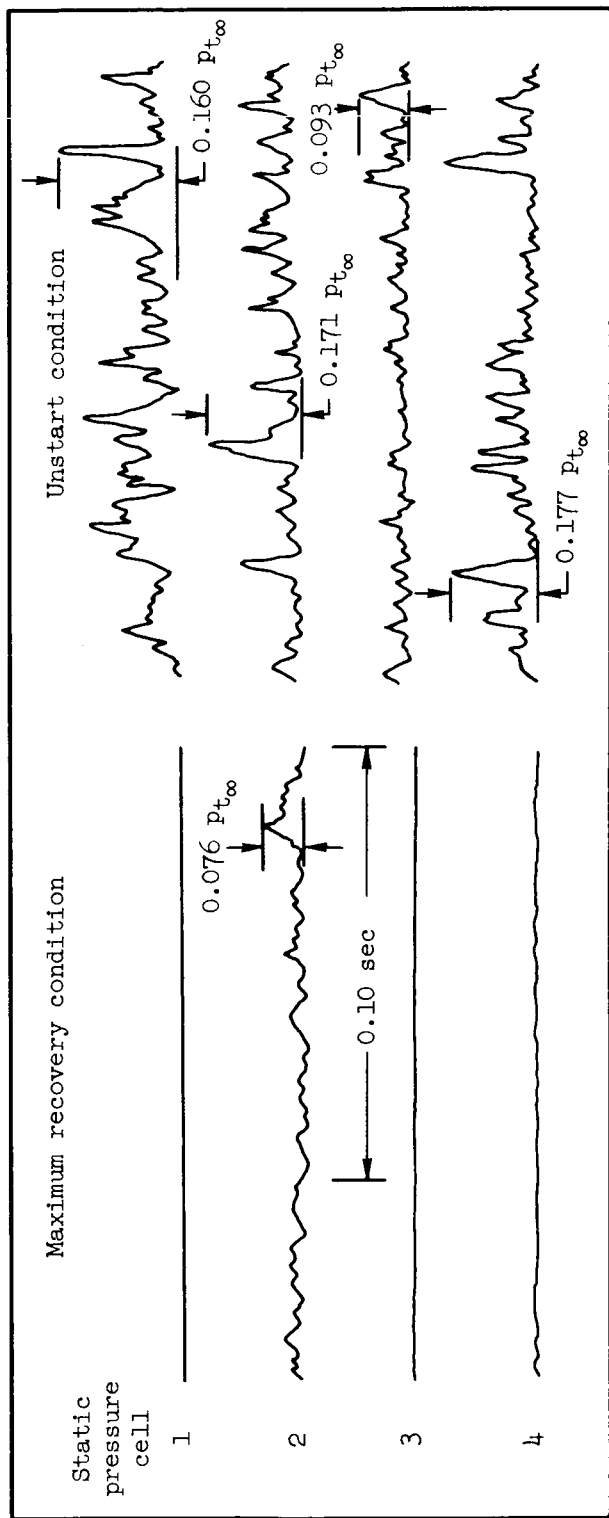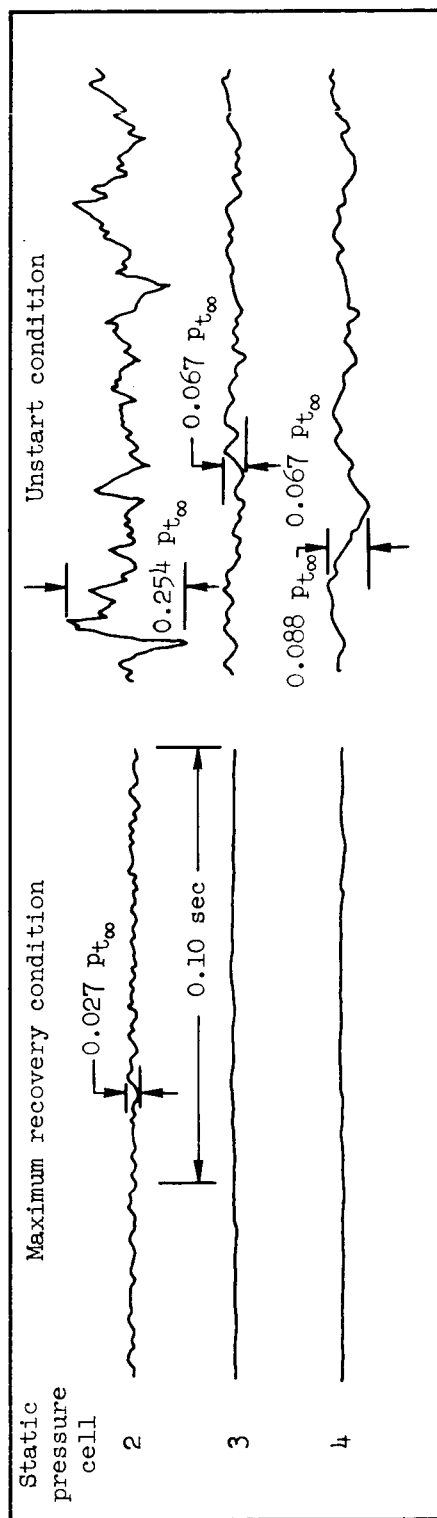$\Delta p_{t_2} = 0.0787$

(d) $\bar{p}_{t_2}/p_{t_\infty} = 0.900$

Figure 25.- Engine-face total-pressure contours; configuration 80 VRF, $M_\infty = 3.0$, $\alpha = 0°$.

(a) Standard diffuser.

(b) Short diffuser.

Figure 26.- Static-pressure unsteadiness; $M_\infty = 3.0$, $\alpha = 0°$.